Cytosolic sodium accumulation is a cellular danger signal triggering endocytic dysfunction and NLRP3 inflammasome activation

Matthew S.J. Mangan[1,2*], Anil Akbal[1], Sophie Rivara[1], Gabor Horvath[1], Philipp Walch[3,4], Jan Hegermann[5], Romina Kaiser[1], Fraser Duthie[1], Joel Selkrig[6], Ralf Gerhard[7], Dagmar Wachten[1], and Eicke Latz[1,2,8,9]

Affiliations:

1. Institute of Innate Immunity, University Hospital Bonn, University of Bonn, 53127 Bonn, Germany.
2. German Center for Neurodegenerative Diseases, 53127, Bonn, Germany.
3. European Molecular Biology Laboratory (EMBL), Genome Biology Unit, 69117 Heidelberg, Germany
4. Heidelberg University, Faculty of Biochemistry, 69120 Heidelberg, Germany
5. Institute of Functional and Applied Anatomy, Research Core Unit Electron Microscopy, OE8840, Hannover Medical School, 30625, Hannover, Germany.
6. Institute for Medical Microbiology, RWTH University Hospital, 52074 Aachen, Germany
7. Institute of Toxicology, Hannover Medical School, 30625 Hannover, Germany.
8. Deutsches Rheuma Forschungszentrum Berlin (DRFZ), 10117, Berlin, Germany.
9. Department of Infectious Diseases & Immunology, UMass Medical School, Worcester, MA 01605, USA.

*Corresponding author. Email: matthew.mangan@ukbonn.de

Abstract

Detection of internalized bacterial toxins and particulate matter within the endo/lysosomal system is essential for the response to cellular intoxication and damage. We reveal that large clostridial toxins, including toxin B from *Clostridioides difficile*, monosodium urate and silica crystals, activate the NLRP3 inflammasome by enabling translocation of sodium from the endo/lysosomal system to the cytosol in human macrophages. Sodium accumulation activates NLRP3 through two distinct mechanisms: Sodium triggers cell swelling and subsequent potassium efflux, while concurrently, it inhibits endocytic trafficking by preventing osmotic resolution of endocytic vesicles. As cytosolic sodium influx and inhibition of endocytic trafficking were also mediated by non-particulate NLRP3 activators ATP and ouabain, our findings illustrate that accumulation of cytosolic sodium is a common danger signal to activate the NLRP3 inflammasome.

Introduction

The endo/lysosomal system serves as the entry route for noxious molecules, including bacterial toxins, pathogens, and particulate matter, many of which perturb endocytic membranes to enter the cytoplasm (*1–3*). Understanding whether these perturbations are detected by the cell and how, remains poorly understood, particularly in the absence of gross damage or rupture to the endo/lysosomal system. An important group of disease-causing toxins that gain entry to the cytoplasm through the endosomal system are the large clostridial toxins (LCT) (*4*). These include toxin B (TcdB) and toxin A (TcdA) from *Clostridioides difficile*, which, solely through expression of these toxins, causes colitis and in some cases sepsis (*5*). Our previous work revealed that TcdB activates the NLRP3 inflammasome in human, monocyte-derived macrophages (hMDM) (*6*). NLRP3 inflammasome activation is a two-step process: It first requires exposure to a Toll-like receptor (TLR) ligand to prime the cell, including induction of NLRP3 expression, and second, an 'activation' step, which triggers inflammasome assembly. The latter is triggered by diverse cellular stresses, including lysosomal damage, but the subsequent cellular events required for NLRP3 activation remain unclear. A decrease in the intracellular potassium concentration is considered essential for many NLRP3 activators (*7*). Additionally, NLRP3 activation is thought to require disruption of the trans-Golgi network (TGN) or endocytic trafficking (*8*), though it is unclear how physiologically relevant NLRP3 stimuli would trigger dysfunction of either system, as these studies were mostly limited to activation of NLRP3 by small molecules and ionophores (*9*, *10*).

Here, we sought to understand how NLRP3 is activated by TcdB in hMDM. During intoxication, TcdB is internalized by receptor-mediated endocytosis, undergoes a

confirmational change at acidic pH (~5.2), inserts into the endo/lysososomal membrane, and translocates to the cytosol (*11*). The protease domain of TcdB cleaves and releases the glycosyltransferase domain of the toxin into the cytosol, where it inactivates RhoA/B/C, Rac1/2/3, and Cdc42 (*11*) (Fig. 1A). To determine which steps are required for NLRP3 activation, we treated LPS-primed hMDM with a series of TcdB mutants, as well as bafilomycin A1 (BafA1), an inhibitor of the vacuolar ATPase that blocks endosomal acidification. NLRP3 activation was assessed by measuring IL-1β release (Fig. 1B, Fig S1A).

Results

Large clostridial toxins activate NLRP3 by structural perturbation of the endolysosomal membrane

We determined that TcdB lacking the C-terminal combined-repetitive oligopeptides (CROP) domain, which enables receptor-mediated internalization (*12*), failed to activate NLRP3 (Fig. 1C). Similarly, pretreatment with BafA1 also prevented TcdB-mediated NLRP3 activation (Fig. 1D). This was not a general effect on NLRP3 activation as BafA1 had no impact on NLRP3 activation by nigericin, an ionophore that mediates K^+/H^+ exchange (Fig. 1D). These results indicated that TcdB required insertion into the endo/lysosomal membrane and translocation into the cytosol to activate NLRP3. To confirm this, we assessed glucosylation of Rac2/3 by TcdB, which only occurs upon translocation to the cytosol. We used an anti-Rac1/2/3 antibody that fails to recognize its epitope after glucosylation by TcdB (*13*). Compared to TcdB, both the TcdB CROP

mutant, which is unable to bind to the CSPG4 receptor (Fig. S1B) and inhibition of vacuolar acidification by BafA1 (Fig. S1C) prevented modification of Rac2/3, confirming that insertion into the endo/lysosomal membrane and translocation into the cytosol is required for TcdB-mediated NLRP3 activation. To investigate whether the enzymatic activity of TcdB that is required for inactivation of RhoA/B/C, Rac1/2/3, and Cdc42 is necessary for NLRP3 activation, we generated a TcdB NXN mutant, which lacks the enzymatic activity required for inactivation of RhoA/B/C, Rac1/2/3, and Cdc42. Notably, TcdB NXN showed enhanced NLRP3 activation compared to TcdB WT (Fig. 1E) demonstrating that TcdB-mediated NLRP3 activation was independent of its enzymatic activity. Instead, this suggested that insertion of TcdB into the endo/lysosomal membrane is sufficient to activate NLRP3. It was therefore surprising that the TcdB ΔGTD mutant, which lacks the GTD entirely, but still inserts into the endo/lysosomal membrane, failed to trigger IL-1β secretion (Fig. 1E). This suggested that the GTD may enhance the ability of TcdB to perturb the endo/lysosomal membrane, leading us to reason that a higher concentration of TcdB ΔGTD would be required achieve the same level of NLRP3 activation as seen for TcdB. Accordingly, TcdB ΔGTD at 0.2 mg/ml, a 10-fold higher concentration than TcdB, activated NLRP3 (Fig. 1F). The NLRP3 inhibitor CP-456,773 (also known as MCC950, CRID3) (*14*) inhibited IL-1β release by the TcdB NXN and ΔGTD mutants as well as TcdB WT, confirming that IL-1β release was NLRP3-dependent for all TcdB mutants. These results demonstrated that TcdB-mediated NLRP3 activation required insertion of TcdB into the endo/lysosomal membrane.

LCT contains a highly conserved translocation domain (*4*), leading us to hypothesize that insertion of any LCT into the endo/lysosomal membrane should activate NLRP3.

Detecting the effects of LCT by monitoring the consequence of its cytoplasmic translocation rather than enzymatic activity is advantageous, as LCT exhibit differing substrate specificities (*4*). In comparison, another inflammasome sensor, the Pyrin inflammasome, is triggered by inactivation of RhoA/B/C (*15*). Thus, Pyrin can only be activated by LCT that specifically inhibit RhoA/B/C (*4*). To test whether NLRP3 was a general LCT sensor, we assessed the inflammasome response to TcdB(F), another pathogenic variant of TcdB, previously identified from clinically relevant isolates of *C. difficile,* and to Lethal Toxin from *Paeniclostridium Sordellii* (TscL) (*16*). These toxins have different substrate specificities within the Rho-GTPase family compared to TcdB, as both inactivate Rac2/3 and Cdc42, but neither inactivate RhoA/B/C (Fig. 1G) (*16*). Similar to TcdB, TcdB(F) and TscL triggered CP-456,773-dependent IL-1β secretion in hMDM, demonstrating that they activate the NLRP3 inflammasome (Fig. 1H). We then assessed the inflammasome response to LCT in monocytes. Unlike hMDM, TcdB activates the Pyrin inflammasome in monocytes, but this would not be activated by TcdB(F) or TscL as they do not inhibit RhoA/B/C (*6*). As anticipated, TcdB activated the Pyrin inflammasome, as IL-1β release was blocked by the Pyrin-inhibitor colchicine. In contrast, IL-1β release in response to TcdB(F) and TscL was CP-456,773- and, therefore, NLRP3-dependent (Fig. S1E). This demonstrates that detection of LCT by NLRP3 through endosomal membrane insertion ensures an inflammasome response irrespective of the toxin substrate specificity.

Insertion of LCT, in particular TcdB, into the endo/lysosomal membrane requires a confirmation shift that exposes the transmembrane domain. This occurs at approximately pH 5.2 (*17*), indicating that trafficking to the late endosome/lysosome is required for

NLRP3 activation. To verify this, we inhibited TcdB trafficking to the late endosomes/lysosomes in hMDM using EGA, a compound that blocks toxin trafficking from early to the late endosome (*18*). EGA blocked activation of NLRP3 by TcdB (Fig. S2A), demonstrating that trafficking to the late endosome/lysosome is required for NLRP3 activation. EGA did not affect TNFα secretion, demonstrating NLRP3-priming was unperturbed (Fig. S2B).

Loss of lysosomal integrity caused by crystals and protein aggregates was shown to activate NLRP3 (*7*). We hypothesized that TcdB also causes loss of lysosomal integrity as TcdB-mediated NLRP3 activation required trafficking to the late endosome/lysosomes. We used TcdB NXN for this experiment and subsequent experiments to avoid confounding effects caused by the inhibition of RhoA/B/C, Rac2/3, and Cdc42. We used a BLaER1 human macrophage cell line expressing a galectin-8-mCitrine fusion protein, which binds to carbohydrates in the lumen of damaged endosomes and forms puncta (*19*). BLaER1 cells incubated with TcdB NXN did not exhibit galectin puncta (Fig. S2C), whereas cells treated with LeuLeu-methyl ester, which causes lysosomal damage, displayed large numbers of puncta (Fig. S2C). This is in line with previous reports showing an absence of galectin-3 or -8 puncta at lysosomes of TcdB-treated Hep-2 cells (*20*). We also tested whether TcdB-mediated NLRP3 activation required cathepsin activity, as it was implicated in lysosomal damage-related NLRP3 activation (*2*). However, neither TcdB- nor nigericin-mediated NLRP3 activation was inhibited by the cathepsin inhibitor CA-047Me (Fig. S2D). Surprisingly, silica-dependent NLRP3 activation, which was proposed to be cathepsin-dependent, was only partially inhibited by CA-047Me (Fig.

S2D). These results collectively demonstrate that TcdB does not activate NLRP3 through gross endo/lysosomal damage.

The absence of TcdB-mediated lysosomal damage suggested that the effect of TcdB on the endo/lysosomal compartment was more subtle. It was shown previously in an artificial system that insertion of TcdB into lipid-bilayer membrane enabled movement of monovalent cations across the membrane, demonstrating that TcdB can act as an ion channel (*21*). TcdB-mediated ion translocation required the pH-mediated confirmational shift, but not the GTD enzymatic activity. Additionally, a considerably higher concentration of the TcdB ΔGTD mutant was needed to enable comparable levels of ion movement as TcdB (*21*), mirroring the requirements for NLRP3 activation (Fig. 1E, F). We assessed lysosomal acidification to determine whether TcdB could indeed act as an ion channel. We treated LPS-primed hMDM with TcdB NXN and TcdB ΔGTD at either 20 ng/ml or 1 μg/ml to verify whether any effects observed correlated to NLRP3 activation. Prior to incubation with TcdB, the LPS-primed hMDM were incubated with the NLRP3 inhibitor CP-456,773 to ensure that any effects observed were not the result of NLRP3 inflammasome activation. Lysosomal acidification was measured by pre-loading hMDM with fluorescent dextrans conjugated to pHrodo green to monitor pH, or to Alexa fluor 647 (A647) as a control. LPS-primed hMDM were incubated with TcdB mutants, and the median fluorescence intensity (MFI) for both dextrans was measured. Both showed a vesicular pattern with overlapping signals, demonstrating that they localize to the same compartment (Fig. S2E). TcdB NXN and 1μg/ml TcdB ΔGTD decreased the MFI of pHrodo green, but not of A647, demonstrating that TcdB decreased lysosomal acidification (Fig. S2F) and that this correlated with NLRP3 activation (Fig. 1E, 1F).

We hypothesized that TcdB alters lysosomal acidification by enabling aberrant ion efflux from endo/lysosomes. To test this directly we assessed the non-canonical autophagic response (CASM). CASM is triggered by an increase of the pH in the lumen of endo/lysosomes, most often caused by proton leakage (*22*). This results in conjugation of LC3-I to lipids in the outer leaflet of the endo/lysosomal membrane, converting LC3-I to its lipidated form, LC3-II. We hypothesized that TcdB would trigger CASM by enabling efflux of protons and/or cations from the lumen of endo/lysosomes. Indeed, all TcdB mutants that activated NLRP3, TcdB WT, TcdB NXN, and TcdB ΔGTD at 1μg/ml, caused an increase in LC3B-II when incubated with LPS-primed hMDM (Fig. 1I, S2G), suggesting that TcdB triggered CASM. CASM differs from canonical autophagy as it requires recruitment of the V_1 subunit of the V-ATPase to the V_0 subunit on the endo/lysosomal membrane, which is inhibited by BafA1 (*22*). To determine whether the LC3B-II increase we observed is due to CASM, we incubated LPS-primed hMDM with BafA1 20 min post-addition of TcdB NXN and found that this reduced the TcdB NXN-dependent increase in LC3-II (Fig. 1J, Fig. S2H). We then performed the same experiment and analyzed the distribution of LC3 and LAMP-1, a lysosomal marker, by laser scanning confocal microscopy (LSC). LPS-primed hMDM treated with TcdB NXN exhibited large, LC3+ vesicles and increased LC3 staining on lysosomes, which were absent in the presence of BafA1 (Fig. 1K). This collectively confirms that TcdB triggers CASM, and indicates that it forms an ion channel in the endo/lysosomal compartment.

TcdB triggers NLRP3 activator by sodium-driven potassium efflux

Our data demonstrate that TcdB enables translocation of protons and possibly other monovalent cations from endo/lysosomes to the cytosol, and this correlates with TcdB-mediated NLRP3 activation (Fig. 1E, 1F). In other contexts, a common mechanism of NLRP3 activation is perturbation of the ionic balance of the cytosol (*7*). As the endo/lysosomal system has significantly higher concentrations of sodium as well as protons compared to the cytoplasm (*23*), we hypothesized that TcdB enables translocation of sodium from the endo/lysosomal lumen into the cytosol to trigger NLRP3 activation. We assessed whether TcdB increased cytosolic sodium by loading hMDM with ION Natrium Green-2 (ING-2), a sodium-specific dye, and measured the change of fluorescence intensity across time in individual cells in response to TcdB NXN. hMDM were pre-incubated with CP-456,773 prior to addition of TcdB to ensure any observed effects were not due to activation of NLPR3. LPS-primed hMDM treated with TcdB NXN, but not LPS alone, displayed a sharp increase in ING-2 fluorescence, demonstrating that TcdB NXN triggered an acute increase in cytosolic sodium, rather than a gradual accumulation (Fig. 2A, 2B, Movie S1-4). This correlated with TcdB-mediated modification of Rac2/3 (Fig. S3A) and occurred prior to TcdB-mediated IL-1β release (Fig. S3B). The increase in cytosolic sodium was inhibited by pre-incubation with BafA1 (Fig. 2A, 2B), demonstrating that it required the pH-driven conformational change of TcdB. We then assessed whether TcdB had any effect on the Na^+/K^+ ATPase, which removes sodium from the cytosol. However, we found no significant difference in the activity of the Na^+/K^+ ATPase after TcdB addition, demonstrating that inhibition of the Na^+/K^+ ATPase did not contribute to TcdB-driven Na^+ accumulation in the cytoplasm (Fig. S3C). This demonstrates that TcdB triggers an acute increase in cytosolic sodium concentration by enabling translocation of endo/lysosomal sodium into the cytoplasm.

To determine whether the TcdB-mediated increase in cytosolic sodium was required for NLRP3 activation, we stimulated LPS-primed hMDM with TcdB in balanced salt solution (BSS), substituting NaCl with N-methyl-D-glucamine chloride (NMGCl), a large monovalent cation that maintains osmolarity and membrane potential, but is inefficiently transported by cellular pumps and ion channels (*24*). Substituting Na^+ for NMG^+ largely prevented the TcdB-driven increase in cytosolic Na^+ (Fig. S3D, Movie S5-8). Similarly, substitution of Na^+ with NMG^+ inhibited NLRP3 activation by TcdB in a concentration-dependent manner (Fig. 2C). However, NMG^+ substitution did not prevent TcdB-mediated modification of Rac2/3, demonstrating that it inhibited NLRP3 activation downstream of insertion of TcdB into the endo/lysosomal membrane (Fig. S3E). To ensure that NMG^+ did not generally inhibit downstream inflammasome components such as ASC and caspase-1 we assessed the effect of NMG^+ substitution on activation of the NLRC4 inflammasome activator by its activator Needletox. In contrast to TcdB, NMG^+ substitution did not inhibit NLRC4 inflammasome activation (Fig. 2C), demonstrating that the effect of NMG^+ is specific to TcdB-mediated NLRP3 activation. This collectively demonstrates that the TcdB-mediated increase in cytosolic sodium is casual for NLRP3 activation.

A key role of sodium is to regulate the volume of the cell , and dysregulation of cell volume has been previously linked to NLRP3 activation (*25*). Therefore, we hypothesized that the TcdB-mediated increase in sodium activated NLRP3 by promoting water influx and cell swelling, which in turn triggers potassium efflux, a common trigger for NLRP3 activation. We first assessed whether TcdB triggered cell swelling by measuring the volume of hMDM following incubation with TcdB NXN using a coulther cathode. TcdB NXN

increased the average cell volume of hMDM (Fig. 2D) as well as the percentage of hMDM with a cell volume greater than the median of the control hMDM (Fig. S3F, S3G). This was evident at 30 min and peaked at 45 min, before decreasing again (Fig. 2D, S3F, S3G). The kinetics of the cell volume increase response mimicked the kinetics of sodium influx (Fig. 2A, 2B).

While TcdB triggered cell swelling, it was surprising that a subsequent decrease in volume was not observed, as this decrease was required for hypoosmotic NLRP3 activation (*25*). However, using this measurement method, we could not distinguish small cells from dead cells. Therefore, we assessed hMDM size at 60 min using flow cytometry, including a dye to assess cell viability. Accordingly, LPS-primed hMDM incubated with TcdB NXN and 1μg/ml TcdB ΔGTD decreased in size 60 min post treatment (Fig. 2E, S3H), and required endosomal acidification (Fig. 2F). These mirrored the requirements for NLRP3 activation (Fig. 1D, 1E, 1F). Consistent with our hypothesis, the TcdB-mediated change in cell volume was prevented by substituting Na^+ for NMG^+ (Fig. 2G). This collectively demonstrated that TcdB-dependent elevation in cytosolic sodium drives changes in cell volume.

We next determined whether TcdB-mediated cell swelling was required for NLRP3 activation by incubating LPS-primed hMDM with TcdB in hyperosmotic extracellular media containing an additional 90mM NaCl (215 mM final) to inhibit cell swelling by preventing water influx into the cytosol. Accordingly, both TcdB-driven cell swelling (Fig. 2G) and NLRP3 activation (Fig. 2H) were inhibited. To confirm that this was due to the osmotic effect of NaCl, we also increased the extracellular osmolarity by adding mannitol,

and found that it similarly inhibited TcdB-mediated NLRP3 activation (Fig. S3I). This was specific to TcdB, as 215 mM NaCl had no effect on NLRP3 activation by nigericin (Fig. 2H). Both 215 mM NaCl and mannitol did not alter TcdB-mediated Rac2/3 modification (Fig. S3J, S3K). These results demonstrate that TcdB activates NLRP3 by triggering cell swelling through an increase in cytosolic sodium.

In other contexts, cell swelling activated NLRP3 by triggering subsequent decrease in cytosolic potassium (*25*, *26*). Thus, we assessed the [K^+] in hMDM following incubation with TcdB NXN and found that it triggered a decrease in cytosolic [K^+] (Fig. 2J). Furthermore, increasing extracellular [KCl] inhibited TcdB-mediated NLRP3 activation of LPS-primed hMDM in a concentration-dependent manner (Fig. 2K), suggesting that TcdB-mediated NLRP3 activation also required potassium efflux. Increased [KCl] had no effect on modification of Rac2/3 by TcdB, demonstrating this effect was downstream of TcdB-mediated insertion into the endo/lysosomal membrane (Fig. S3L). Increased [KCl] was specific to NLRP3 inflammasome activation, as it did not inhibit activation of NLRC4 by its activator, Needletox (Fig. 2K). This demonstrates that the TcdB-mediated increase in cytosolic sodium drives NLRP3 activation through a cell swelling-dependent decrease in cytosolic potassium.

Macropinocytosis is required for TcdB-mediated NLRP3 activation

Our results showed that TcdB-mediated translocation of endo/lysosomal sodium into the cytosol was the initiating event triggering NLRP3 activation. Notably, exchanging extracellular Na^+ for NMG^+ reduced the TcdB-mediated increase in cytosolic sodium (Fig. S3D) as well as NLRP3 activation (Fig. 2C). This indicated that ongoing uptake of Na^+

from the extracellular media into the cytosol was required for the TcdB-mediated increase in cytosolic sodium. One mechanism for the internalization of extracellular Na^+ is macropinocytosis, a specialized form of endocytosis characterized by the non-specific uptake of large amounts of extracellular fluid (*27*). hMDM perform macropinocytosis prolifically and, unlike other cells, do so constitutively (*28*). Therefore, we targeted different processes required for macropinosome formation using pharmacological inhibitors: EIPA, which inhibits Na^+/H^+ exchange, LY-294002, a class I PI3K inhibitor, two inhibitors of actin rearrangement, jasplakinolide and latrunculin B, and NPS2143, an inhibitor of the calcium sensing GPCR (CaSR), which inhibits constitutive macropinocytosis in hMDM (*29*) (Fig. 3A). All compounds inhibited TcdB-mediated IL-1β release (Fig. 3B), but did not inhibit activation of NLRP3 by nigericin (Fig. 3B). Similarly, all compounds inhibited macropinocytosis as measured by uptake of a 70 kDa Oregon green-conjugated dextran (Fig. S4A), but did not inhibit entry of TcdB into the cytoplasm, as measured by modification of Rac2/3 (Fig. S4B). We confirmed these results by knocking down the CaSR (Fig. S4C). CasR knock down reduced macropinocytosis in the hMDM (Fig.S4D) and similarly inhibited NLRP3 activation by TcdB, but had no effect on TNFα secretion (Fig. 3D).

To test whether inhibition of macropinocytosis prevented TcdB-driven NLRP3 activation by reducing the increase in cytosolic sodium, we pre-incubated hMDM with the macropinocytosis inhibitors, then assessed ING-2 fluorescence following addition of TcdB NXN. Inhibiting macropinocytosis reduced the velocity and amplitude of the TcdB-mediated increase in cytosolic sodium, resulting in a decrease in the fraction of cells with higher ING-2 intensity at 30 min post-addition of TcdB (Fig. 3E, Movie S9-13). However,

it did not reduce ING-2 intensity to the level of hMDM treated with LPS alone, demonstrating that macropinocytosis is partially required for the TcdB-driven increase in cytosolic sodium, but that other processes also contribute to it (Fig. 3E). Furthermore, LY-294002 and NPS2143 prevented the TcdB-mediated increase in cell volume, confirming that macropinocytosis-dependent Na^+ internalization is required to trigger TcdB-dependent cell swelling (Fig. S4E). The effects of macropinocytosis on TcdB-driven NLRP3 activation were not due to altered uptake of TcdB, as, with the exception of latrunculin B, macropinosome inhibitors did not decrease TcdB uptake (Fig. S4F). Similarly, we found no evidence of TcdB inserting directly into the membranes of macropinosomes, as TcdB-dependent CASM, measured by LC3B-II levels, was also unchanged by macropinosome inhibitors (Fig. S4G). There results demonstrate that macropinocytosis is required for TcdB-mediated NLRP3 activation by contributing to the increase in cytosolic sodium required to trigger subsequent cell swelling.

Cytosolic sodium increase is required for NLRP3 activation by crystalline particulates, ATP and Na^+/K^+ ATPase inhibition

Our data demonstrated that translocation of sodium from the endocytic system to the cytosol was sufficient to trigger NLRP3 activation. Other noxious molecules, including mono-sodium urate (MSU) and silica crystals activate NLRP3 by damaging endo/lysosomal membranes (*2*). This was considered to be entirely cathepsin dependent, however a combined knock-out of 5 cathepsins only partially decreased NLRP3 activation caused by lysosomal rupture (*30*). To determine if crystal-mediated lysosomal damage enables sodium translocation, we assessed ING-2 fluorescence in hMDM treated with MSU in Na^+- or NMG^+-containing BSS. Similar to TcdB, MSU triggered a sharp increase

in ING-2 fluorescence, indicative of acute increase in cytosolic sodium that was absent in the presence of NMG^+ BSS (Fig. 4A). We then assessed whether the MSU-dependent increase in cytosolic sodium was required for NLRP3 activation and determined that substitution of even half of the extracellular Na^+ for NMG^+ containing BSS was sufficient to prevent activation of NLRP3 (Fig. 4B). Treatment of hMDM with silica crystals similarly triggered sodium translocation (Fig. S5A) and also required extracellular sodium, though this was to a lesser degree than observed with MSU (Fig. S5B). These results demonstrate that translocation of sodium from the endo/lysosomal system to the cytosol is a common requirement for activation of NLRP3 by particulate matter.

In addition to sodium translocation from the endo/lysosomes, many NLRP3 activators, including ATP and pore-forming toxins, activate NLRP3 by permeabilizing the plasma membrane to ions (*31*). We hypothesized that this, similar to permabilization of the endo/lysosomal system, result in an acute influx of extracellular sodium into the cell accompanied by a potassium efflux. To test this, we stimulated hMDM with ATP, which opens the P2X7 receptor, enabling movement of K^+, Na^+, and Ca^{2+} across the plasma membrane. We found that ATP indeed triggered a rapid cytosolic sodium influx (Fig. 4C). Substitution of extracellular sodium reduced ATP-mediated IL-1β release (Fig. 4D), demonstrating that sodium influx is a partial requirement for NLRP3 activation by ATP.

All NLRP3 activators that we have investigated so far caused an increase in cytosolic sodium influx by permeabilizing the endo/lysosomal or plasma membranes to ions. However, sodium also constantly enters the cytosol under homeostatic conditions, where it will then accumulate if it is not efficiently removed by the Na^+/K^+ ATPase. Indeed,

inhibition of the Na^+/K^+ ATPase by ouabain or potassium-free media also activates NLRP3 (*7*). Macropinocytosis is a key import pathway for sodium, as shown in our previous experiments, and we hypothesized that it would similarly contribute to NLRP3 activation by Na^+/K^+ ATP inhibition. We determined that inhibition of macropinocytosis by LY-294002 and NPS214 markedly decreased IL-1β release and caspase-1 activation in LPS-primed hMDM incubated with the Na^+/K^+ ATP inhibitor ouabain (Fig. 4E), as did the NLRP3 inhibitor CP-456,773 (Fig. 4E). To confirm the role of macropinocytosis, we generated pooled knock-outs of the two-pore channel 1 and 2 (TPC1 and TPC2), which are partially required for sodium efflux from macropinosome (*32*). We achieved an average knock out efficiency of 24.8% for TPCN1 and 72% for TPCN2 (Fig. S5C). Knocking out TPC1 and TPC2 partially reduced ouabain-induced NLRP3 activation compared to control hMDM (Fig. 4F), indicating that sodium influx through macropinosomes contributes to NLRP3 activation by ouabain.

Cytosolic sodium increase triggers activation of NLRP3 by perturbing osmotic regulation of endosomal trafficking

Our data established that cytosolic sodium accumulation is a common event required for NLRP3 activation by a diverse range of stimuli. Recent studies indicated that NLRP3 activation required inhibition of endosomal trafficking (*10*, *33*). However, these studies investigated this using ionophores and small molecules that can act directly on the endocytic system (*9*, *10*). In contrast, all known physiologically relevant triggers of NLRP3 do not act directly on endocytic trafficking. Therefore, it is unclear whether they inhibit endocytic trafficking and if so, how they would inhibit it. Notably, endocytic trafficking is dependent on the passive efflux of sodium and chloride from the endosomal lumen into

the cytosol (*23*). Our data demonstrated that the TcdB-mediated increase in cytosolic sodium precedes the decrease in cytosolic potassium. Therefore, we hypothesized that the increase in cytosolic sodium mediated by TcdB and other NLRP3 activators would enable NLRP3 activation by preventing sodium efflux from endosomes and thereby inhibit endocytic trafficking.

To test this, we assessed whether TcdB inhibited endosomal trafficking using a pulse chase assay with A647-labelled transferrin (Tfn-A647). Trafficking of the Tfn-Tfn receptor complex is clathrin-dependent, and following internalization the receptor is transported to the early endosome before being recycled back to the plasma membrane (Fig. S6A). Inhibition of endocytic trafficking would thus result in an increased proportion of hMDM with Tfn-A647-positive vesicles. LPS-treated hMDM were pulsed for 10 min with Tfn-A647 at 25 min post TcdB NXN treatment, then assessed for the number of cells with Tfn-A647-positive (Tfn^+) vesicles at 10 min intervals (Fig. 5A). We determined that a proportion of hMDM incubated with TcdB NXN contained Tfn^+ vesicles even after a 30 min chase period (Fig. 5A), which were not present in the LPS-treated control (Fig. 5A), indicating that TcdB inhibited endocytic trafficking. Furthermore, Tfn trafficking was inhibited in hMDM treated with 1 μg/ml TcdB ΔGTD but not 20 ng/ml, correlating with TcdB-mediated cell swelling and NLRP3 activation (Fig. S6B). Tfn +ve vesicles in the TcdB-treated hMDM colocalized with Rab5, a marker of the early endosome (Fig. 5B). To confirm that the increase in Tfn^+ hMDM was due to inhibition of endocytic trafficking and not differential Tfn uptake, we assessed Tfn-A647 binding and found it was unaffected by TcdB (Fig. S6C). These results demonstrate that TcdB inhibits endosomal trafficking of Tfn at the

level of the early endosome, correlating with both an increase in cytosolic sodium and NLRP3 activation.

To confirm that TcdB generally inhibited endocytic trafficking, we assessed endocytic transport of Alexafluor-594-labeled cholera toxin subunit B (CtxB). In contrast to Tfn, CtxB trafficking is clathrin-independent, and it is transported to the cytosol rather than being re-externalized (Fig. S6D). Incubation with TcdB NXN increased the proportion of hMDM with CtxB-positive vesicles ($CtxB^+$) compared to LPS-primed hMDM (Fig. S6E). This was not due to differential uptake of CtxB, as the overall amount of CtxB taken up, as measured by the integrated intensity of the cell, was unchanged by TcdB (Fig. S6E). $CtxB^+$ vesicles colocalized with Rab5 (Fig. S6F). This collectively demonstrates that TcdB also inhibits endocytic trafficking of CtxB at the level of the early endosome, and so is a general inhibitor of endocytic trafficking.

Our results revealed a strong correlation between TcdB-mediated inhibition of endocytic trafficking and NLRP3 activation. To confirm this, we correlated trafficking inhibition with a marker of inflammasome activation, ASC-speck formation (*34*). As expected, only LPS-primed hMDM incubated with TcdB NXN displayed ASC specks, with around 10% of the population responding (Fig. 5C). Of these, almost all hMDM with an ASC speck were Tfn^+ (Fig. 5C), demonstrating a strong correlation between NLRP3 activation and endosomal trafficking inhibition.

The TcdB-driven increase in cytosolic sodium should disrupt endocytic trafficking by preventing sodium movement from the endosomal lumen to the cytosol, thus inhibiting

the movement of water. We tested this by assessing the impact of TcdB on the size reduction of macropinosomes. Macropinosomes reduce in size following passive efflux of sodium and chloride, which then triggers water efflux (Fig. 5D) (*23*). Thus, if the TcdB-mediated increase in cytosolic Na^+ disrupts sodium efflux, macropinosomes will not decrease in size. Assessing the shrinkage of macropinosomes is advantageous compared to other endosomal vesicles as they are sufficiently large to accurately measure their change in size. We stimulated macropinosome formation in hMDM by pulsing them with M-CSF in the presence of a 70 kDa fluorescent dextran for 5 min. Macropinosome shrinkage was assessed by the size reduction and the increase in dextran intensity as it is concentrated in the lumen of the macropinosome (*32*). Strikingly, macropinosomes formed in LPS-primed hMDM incubated with TcdB failed to reduce in volume, and displayed no increase in fluorescence intensity (Fig. 5E, S7A, Movie S14). In contrast, macropinosomes formed in the LPS-primed hMDM reduced in size and increased in fluorescence intensity across the 10 min time period as anticipated (Fig. 5E, S7A, Video S15), demonstrating that TcdB inhibited the size reduction of macropinosomes. To confirm that this was due to inhibition of water efflux from the lumen of the macropinosomes, we pulsed the dextran-loaded, LPS- and TcdB NXN- treated hMDM with hyperosmotic BSS to induce water efflux from the macropinosomes. Accordingly, pulsing TcdB-treated hMDM with hyperosmotic BSS caused the macropinosomes to reduce in size (Fig. S7B, Movie S16-17), confirming that the macropinosomes failed to shrink due to retention of water in the lumen of macropinosomes. To assess the presence of unresolved macropinosomes independently of dextran loading, we assessed the LPS-primed hMDM treated with TcdB NXN by transmission electron microscopy (TEM) and found they displayed large vacuolar

structures lacking electron density which were absent in the LPS-primed hMDM, (Fig. 5F), indicating that they are macropinosomes. These results demonstrate that TcdB inhibits the size reduction of macropinosomes by preventing their osmotic resolution.

A consequence of retention of sodium, and therefore water, in the endosomal lumen is a failure to decrease endosomal membrane tension, which is the requirement for endocytic trafficking (*35*). We assessed endocytic membrane tension using the early endosomal flipper dye (EE-flipper), which integrates into endosomal membranes and changes fluorescence lifetime based on endosomal membrane tension (*36*). We first measured EE flipper fluorescence lifetime changes in response to mannitol, which decreases endosomal membrane tension, and monensin, which increases it. As anticipated, mannitol decreased the fluorescence lifetime of EE flipper (Fig. S7C), while monensin increased it (Fig. S7D). We then assessed whether TcdB altered endosomal membrane tension in LPS-primed hMDM and found that incubation with TcdB consistently resulted in an increase in fluorescence lifetime, indicative of increased membrane tension (Fig. 5G, S7E). In contrast, there was no change in fluorescence lifetime in the hMDM incubated with LPS alone (Fig. 5G, S7E). These results collectively demonstrate that TcdB inhibits endosomal trafficking by preventing osmotic resolution of endosomes and macropinosomes.

An increase in cytosolic sodium was a common effect for other NLRP3 stimuli we had tested, suggesting that it might be a common mechanism to disrupt endocytic trafficking and enable NLRP3 activation. Therefore, we assessed Tfn-A647 trafficking in response to ATP, ouabain, and K^+ free media. Notably, all three increased the number of hMDM

with Tfn^+ vesicles (Fig. 5H, S8A). This was due to inhibition of endocytic trafficking, Tfn-A647 binding was unaffected (Fig. S8B). Consistent with our previous findings, treating LPS-primed hMDM with ATP, ouabain and K^+ free media also increased endosomal membrane tension (Fig. 5I, S8C), while in all cases the LPS-primed hMDM showed no change (Fig. 5I). This demonstrates that endocytic trafficking is generally inhibited by NLRP3 activators through perturbation of osmotic resolution of endosomes.

Discussion

In this study, we demonstrate that accumulation of cytosolic sodium is a danger signal that activates the NLRP3 inflammasome, which, in turn, triggers release of pro-inflammatory cytokines, translating cytosolic sodium accumulation into an inflammatory response. The acute increase in cytosolic sodium activated NLRP3 through at least two distinct pathways (Fig. S9): It perturbed the ionic balance of the cytosol, triggering water influx, cell swelling and a subsequent potassium efflux. Independently, it inhibited endosomal trafficking by preventing water efflux and a loss of membrane tension. In addition to these two processes, it is possible that sodium also has a direct effect on NLRP3 itself. Furthermore, sodium might also have a direct effect on NLRP3 by regulating NLRP3 oligomer formation, which is thought to be required for its activation by some activators (*37*, *38*).

Detection of aberrantly translocated mitochondrial and genomic DNA, as well as RNA, has been shown to activate innate immune sensors when translocated to the cytosol under stress or infection (*39*). Our study data demonstrates that aberrant ion translocation

is a similar danger signal, as permeabilization of the endo/lysosomes for sodium was sufficient to activate NLRP3. In comparison to larger molecules, ions are a more effective way to “detect” permeabilization or ‘leakiness’ of endo/lysosomal membranes, as they are present in high abundance, are sufficiently small to be released both early and easily, and can rapidly diffuse into the cytosol. Detection of sodium also enables a graded response, as NLRP3 activation will only occur if the increase is sufficiently large and acute that it impacts cell volume. Of note, recent studies have demonstrated that STING also triggers an inflammatory response by enabling ion translocation (*40*), suggesting that ion translocation as a danger signal may be more prevalent than previously anticipated.

Our study demonstrates a physiological role for NLRP3 in pathogen detection, which has been controversial (*41*). Translocation of pathogen-derived toxins and effectors across the endo/lysosomal membrane is a highly conserved mechanism used to access the cytosol (*42*). Monitoring insertion of these toxins/effectors by detecting the subsequent sodium translocation is advantageous as it enables detection of a wide range of effectors regardless of their other activities. In the case of LCT, NLRP3 is activated by LCT insertion into the endo/lysosome membrane, which is conserved amongst the entire LCT family. Notably, the TcdB translocation domain is conserved across 1104 bacterial proteins expressed by both pathogenic and commensal bacteria proteins, with many proteins also containing toxin-like effector domains (*43*). This suggests that the TcdB translocation domain is a common delivery system for bacterial effectors with the potential to disrupt endo/lysosomal membranes (*17*). A plethora of other pathogenic molecules including viroporins produced by virus including the influenza virus and SARS-COV-2, as well as bacterial toxins including listeria lysin O and VacA, can potentially enable ion translocation

to the cytoplasm. This extends to structurally unrelated toxins, including C3-like toxins that enter the cell by triggering lysosomal swelling and subsequent disruption (*44*). Further research is required to determine in whether these molecules trigger sufficient ion efflux activate NLRP3, but implies that NLRP3 may be important for sensing a wide range of pathogenic molecules, and is important for monitoring the integrity of the endocytic system.

Our study contrasts to previous studies indicating that cathepsins are required for NLRP3 activation downstream of lysosomal disruption (*2*, *30*). In hMDM, TcdB-mediated NLRP3 activation was cathepsin independent, while cathepsin inhibition only caused a minor reduction in silica-mediated NLRP3 activation. The differences between our study and previously published work could be due to differences between species, as most studies assessing cathepsin dependence on NLRP3 activation were performed in murine cells (*2*, *30*). Consistent with this, substitution of sodium in BMDM also did not prevent NLRP3 activation by silica crystals as we observe in hMDM (*45*). Cathepsin dependence is also difficult to prove, as they are redundant and cathepsin inhibitors are invariably based on cysteine reactive moieties, and so can inhibit NLRP3 directly (*7*, *30*). Further research will be required to delineate the role of each, though cathepsin release occurring on following greater levels of lysosomal damage may compensate for the absence of sodium, and so may both may be part of a graded response to lysosomal damage.

Macropinocytosis contributed to NLRP3 activation by both TcdB and ouabain, demonstrating that sodium imported by macropinosomes is an important contributor to sensing sodium as a danger signal. Interestingly, a recent study found that

macropinocytosis was required to maintain cytosolic chloride levels in macrophages under steady state conditions (*46*), suggesting that macropinocytosis is a significant import mechanism for ions. For ouabain activation, it is likely that homeostatic sodium efflux from lumen of macropinosomes into the cytoplasm was responsible, as the sodium could not be subsequently removed from the cytoplasm. The role of macropinocytosis in TcdB-mediated cytosolic sodium accumulation and NLRP3 activation is less clear. Macropinocytosis did not enable acute cytosolic sodium increase by altering TcdB uptake and we found no evidence that it inserts directly into the membranes of macropinosomes. The increase in cytosolic sodium was acute, suggesting that homeostatic sodium efflux from macropinosomes into the cytoplasm also does not contribute. Rather, the sharp increase in cytosolic sodium suggested that the sodium in the endo/lysosomal system was already sufficient to drive NLRP3 activation. This indicates that macropinocytosis rather regulates the amount or concentration of sodium in the endo/lysosomal system, and inhibition of this process prior to TcdB reduces the amount of sodium in the endo/lysosomal system that can enter the cell. However, further experimentation will be required to verify this. This has implications for detection of LCT through sodium influx, as all LCT inhibit Rac1/2/3 (*47*), and subsequently inhibit macropinocytosis once the effector domain reaches the cytosol. As such, NLRP3 activation of LCT will depend on how much toxin is internalised, and whether it triggers sodium translocation to the cytosol prior to inhibition of Rac1/2/3.

Inhibition of endocytic trafficking, also shown through dispersal of the TGN marker TGN46, has been implicated in NLRP3 activation (*9*, *10*). However, this has been almost exclusively investigated using ionophores or small molecules that directly disrupt ion

gradients across endosomal and TGN membranes. These compounds contrast with physiologically relevant NLRP3 activators that permeabilize the plasma membrane (PM) or lysosomal membranes, or prevent potassium uptake (*31*). As they do not act directly on the TGN or endocytic system, it was unclear how these activators could perturb either of these compartments. Our study demonstrates that NLRP3 activators TcdB, ATP, ouabain, and K^+ free media all inhibit endocytic trafficking by increasing cytosolic sodium. This increase disrupts passive sodium efflux from the endosomal lumen, preventing water efflux and the loss of endosomal membrane tension required for onward trafficking (*23*). This finding has implications beyond NLRP3 activation, as efficient endocytic trafficking is essential for many cellular functions. Thus, our study demonstrates mechanisms through which cytosolic sodium accumulation affects cellular functions, and that a sodium overload can act as a danger signal to inhibit endocytic trafficking and facilitate activation of the NLRP3 inflammasome.

References

1. M. Herb, A. Gluschko, A. Farid, M. Krönke, When the Phagosome Gets Leaky: Pore-Forming Toxin-Induced Non-Canonical Autophagy (PINCA). *Front. Cell. Infect. Microbiol.* **12**, 834321 (2022).

2. V. Hornung, F. Bauernfeind, A. Halle, E. O. Samstad, H. Kono, K. L. Rock, K. A. Fitzgerald, E. Latz, Silica crystals and aluminum salts activate the NALP3 inflammasome through phagosomal destabilization. *Nat Immunol* **9**, 847–856 (2008).

3. B. Geny, M. R. Popoff, Bacterial protein toxins and lipids: pore formation or toxin entry into cells. *Biol. Cell* **98**, 667–678 (2006).

4. J. Schirmer, K. Aktories, Large clostridial cytotoxins: cellular biology of Rho/Ras-glucosylating toxins. *Biochimica Et Biophysica Acta Bba - Gen Subj* **1673**, 66–74 (2004).

5. W. K. Smits, D. Lyras, D. B. Lacy, M. H. Wilcox, E. J. Kuijper, Clostridium difficile infection. *Nat Rev Dis Primers* **2**, 16020 (2016).

6. M. S. J. Mangan, F. Gorki, K. Krause, A. Heinz, A. Pankow, T. Ebert, D. Jahn, K. Hiller, V. Hornung, M. Maurer, F. I. Schmidt, R. Gerhard, E. Latz, Transcriptional licensing is required for Pyrin inflammasome activation in human macrophages and bypassed by mutations causing familial Mediterranean fever. *PLOS Biol.* **20**, e3001351 (2022).

7. M. S. J. Mangan, E. J. Olhava, W. R. Roush, H. M. Seidel, G. D. Glick, E. Latz, Targeting the NLRP3 inflammasome in inflammatory diseases. *Nat Rev Drug Discov* **17**, 588–606 (2018).

8. A. Akbal, A. Dernst, M. Lovotti, M. S. J. Mangan, R. M. McManus, E. Latz, How location and cellular signaling combine to activate the NLRP3 inflammasome. *Cell. Mol. Immunol.* **19**, 1201–1214 (2022).

9. J. Chen, Z. J. Chen, PtdIns4P on dispersed trans-Golgi network mediates NLRP3 inflammasome activation. *Nature* **564**, 71–76 (2018).

10. Z. Zhang, R. Venditti, L. Ran, Z. Liu, K. Vivot, A. Schürmann, J. S. Bonifacino, M. A. D. Matteis, R. Ricci, Distinct changes in endosomal composition promote NLRP3 inflammasome activation. *Nat. Immunol.* **24**, 30–41 (2023).

11. K. Aktories, C. Schwan, T. Jank, Clostridium difficile Toxin Biology. *Annu Rev Microbiol* **71**, 1–27 (2016).

12. P. Chen, J. Zeng, Z. Liu, H. Thaker, S. Wang, S. Tian, J. Zhang, L. Tao, C. B. Gutierrez, L. Xing, R. Gerhard, L. Huang, M. Dong, R. Jin, Structural basis for CSPG4 as a receptor for TcdB and a therapeutic target in Clostridioides difficile infection. *Nat Commun* **12**, 3748 (2021).

13. H. Genth, J. Huelsenbeck, B. Hartmann, F. Hofmann, I. Just, R. Gerhard, Cellular stability of Rho-GTPases glucosylated by Clostridium difficile toxin B. *Febs Lett* **580**, 3565–3569 (2006).

14. R. C. Coll, A. A. B. Robertson, J. J. Chae, S. C. Higgins, R. Muñoz-Planillo, M. C. Inserra, I. Vetter, L. S. Dungan, B. G. Monks, A. Stutz, D. E. Croker, M. S. Butler, M. Haneklaus, C. E. Sutton, G. Núñez, E. Latz, D. L. Kastner, K. H. G. Mills, S. L. Masters, K. Schroder, M. A. Cooper, L. A. J. O'Neill, A small-molecule inhibitor of the NLRP3 inflammasome for the treatment of inflammatory diseases. *Nat. Med.* **21**, 248–255 (2015).

15. H. Xu, J. Yang, W. Gao, L. Li, P. Li, L. Zhang, Y.-N. Gong, X. Peng, J. J. Xi, S. Chen, F. Wang, F. Shao, Innate immune sensing of bacterial modifications of Rho GTPases by the Pyrin inflammasome. *Nature* **513**, 237–241 (2014).

16. H. Genth, S. C. Dreger, J. Huelsenbeck, I. Just, Clostridium difficile toxins: More than mere inhibitors of Rho proteins. *Int. J. Biochem. Cell Biol.* **40**, 592–597 (2008).

17. O. E. Kathleen, Z. Zhifen, S.-M. N. Seiji, M. A. Roman, Clostridium difficile toxins A and B: Receptors, pores, and translocation into cells. *Crit Rev Biochem Mol* **52**, 461–473 (2017).

18. E. J. Gillespie, C.-L. C. Ho, K. Balaji, D. L. Clemens, G. Deng, Y. E. Wang, H. J. Elsaesser, B. Tamilselvam, A. Gargi, S. D. Dixon, B. France, B. T. Chamberlain, S. R. Blanke, G. Cheng, J. C. de la Torre, D. G. Brooks, M. E. Jung, J. Colicelli, R. Damoiseaux, K. A. Bradley, Selective inhibitor of endosomal trafficking pathways exploited by multiple toxins and viruses. *Proc National Acad Sci* **110**, E4904–E4912 (2013).

19. T. L. M. Thurston, M. P. Wandel, N. von Muhlinen, Á. Foeglein, F. Randow, Galectin 8 targets damaged vesicles for autophagy todefend cells against bacterial invasion. *Nature* **482**, 414–418 (2012).

20. C. Klepka, M. Sandmann, H. Tatge, M. Mangan, A. Arens, D. Henkel, R. Gerhard, Impairment of lysosomal function by Clostridioides difficile TcdB. *Mol. Microbiol.* **117**, 493–507 (2022).

21. H. Barth, G. Pfeifer, F. Hofmann, E. Maier, R. Benz, K. Aktories, Low pH-induced Formation of Ion Channels by Clostridium difficile Toxin B in Target Cells*. *J Biol Chem* **276**, 10670–10676 (2001).

22. J. Durgan, O. Florey, Many roads lead to CASM: Diverse stimuli of noncanonical autophagy share a unifying molecular mechanism. *Sci. Adv.* **8**, eabo1274 (2022).

23. A. Saric, S. A. Freeman, Endomembrane Tension and Trafficking. *Frontiers Cell Dev Biology* **8**, 611326 (2021).

24. E. J. Blackstock, G. W. Stewart, The dependence on external cation of sodium and potassium fluxes across the human red cell membrane at low temperatures. *J Physiology* **375**, 403–420 (1986).

25. V. Compan, A. Baroja-Mazo, G. López-Castejón, A. I. Gomez, C. M. Martínez, D. Angosto, M. T. Montero, A. S. Herranz, E. Bazán, D. Reimers, V. Mulero, P. Pelegrín, Cell Volume Regulation Modulates NLRP3 Inflammasome Activation. *Immunity* **37**, 487–500 (2012).

26. V. Pétrilli, S. Papin, C. Dostert, A. Mayor, F. Martinon, J. Tschopp, Activation of the NALP3 inflammasome is triggered by low intracellular potassium concentration. *Cell Death Differ* **14**, 1583–1589 (2007).

27. J. Mercer, A. Helenius, Gulping rather than sipping: macropinocytosis as a way of virus entry. *Curr Opin Microbiol* **15**, 490–499 (2012).

28. J. Canton, Macropinocytosis: New Insights Into Its Underappreciated Role in Innate Immune Cell Surveillance. *Front Immunol* **9**, 2286 (2018).

29. J. Canton, D. Schlam, C. Breuer, M. Gütschow, M. Glogauer, S. Grinstein, Calcium-sensing receptors signal constitutive macropinocytosis and facilitate the uptake of NOD2 ligands in macrophages. *Nat Commun* **7**, 11284 (2016).

30. G. M. Orlowski, J. D. Colbert, S. Sharma, M. Bogyo, S. A. Robertson, K. L. Rock, Multiple Cathepsins Promote Pro–IL-1β Synthesis and NLRP3-Mediated IL-1β Activation. *J. Immunol.* **195**, 1685–1697 (2015).

31. K. V. Swanson, M. Deng, J. P.-Y. Ting, The NLRP3 inflammasome: molecular activation and regulation to therapeutics. *Nat Rev Immunol* **19**, 477–489 (2019).

32. S. A. Freeman, S. Uderhardt, A. Saric, R. F. Collins, C. M. Buckley, S. Mylvaganam, P. Boroumand, J. Plumb, R. N. Germain, D. Ren, S. Grinstein, Lipid-gated monovalent ion fluxes regulate endocytic traffic and support immune surveillance. *Science* **367**, 301–305 (2020).

33. J. Chen, Z. J. Chen, PtdIns4P on dispersed trans-Golgi network mediates NLRP3 inflammasome activation. *Nature* **564**, 71–76 (2018).

34. B. S. Franklin, L. Bossaller, D. D. Nardo, J. M. Ratter, A. Stutz, G. Engels, C. Brenker, M. Nordhoff, S. R. Mirandola, A. Al-Amoudi, M. S. Mangan, S. Zimmer, B. G. Monks, M. Fricke, R. E. Schmidt, T. Espevik, B. Jones, A. G. Jarnicki, P. M. Hansbro, P. Busto, A. Marshak-Rothstein, S. Hornemann, A. Aguzzi, W. Kastenmüller, E. Latz, The adaptor ASC has extracellular and “prionoid” activities that propagate inflammation. *Nat. Immunol.* **15**, 727–737 (2014).

35. V. Mercier, J. Larios, G. Molinard, A. Goujon, S. Matile, J. Gruenberg, A. Roux, Endosomal membrane tension regulates ESCRT-III-dependent intra-lumenal vesicle formation. *Nat Cell Biol* **22**, 947–959 (2020).

36. P. Francesca, M. Vincent, A. Lea, S. Naomi, R. Aurelien, M. Stefan, Fluorescent Membrane Tension Probes for Early Endosomes. *Angew. Chem. Int. Ed.* **60**, 12258–12263 (2021).

37. I. V. Hochheiser, M. Pilsl, G. Hagelueken, J. Moecking, M. Marleaux, R. Brinkschulte, E. Latz, C. Engel, M. Geyer, Cryo-EM structure of the NLRP3 decamer bound to the cytokine release inhibitory drug CRID3. *Biorxiv*, 2021.07.22.453353 (2021).

38. L. Andreeva, L. David, S. Rawson, C. Shen, T. Pasricha, P. Pelegrin, H. Wu, NLRP3 cages revealed by full-length mouse NLRP3 structure control pathway activation. *Cell* **184**, 6299-6312.e22 (2021).

39. K. N. Miller, S. G. Victorelli, H. Salmonowicz, N. Dasgupta, T. Liu, J. F. Passos, P. D. Adams, Cytoplasmic DNA: sources, sensing, and role in aging and disease. *Cell* **184**, 5506–5526 (2021).

40. L. Bingxu, C. J. Rebecca, P. S. Ivan, G. Matteo, F. Ellie, H. Quentin, S. A. Marc, B. C. Paul, I. J. Darrell, H. Nir, Human STING is a proton channel. *Science* **381**, 508–514 (2023).

41. R. Coll, L. O'Neill, K. Schroder, Questions and controversies in innate immune research: what is the physiological role of NLRP3? *Cell Death Discov* **2**, 16019 (2016).

42. J. M. Williams, B. Tsai, Intracellular trafficking of bacterial toxins. *Curr. Opin. Cell Biol.* **41**, 51–56 (2016).

43. K. E. Orrell, M. J. Mansfield, A. C. Doxey, R. A. Melnyk, The C. difficile toxin B membrane translocation machinery is an evolutionarily conserved protein delivery apparatus. *Nat Commun* **11**, 432 (2020).

44. M. Turner, J. Plumb, A. R. Merrill, S. Grinstein, J. Westman, Lysosomal swelling and lysis mediate delivery of C3 toxins to their cytoplasmic targets. *Mol. Microbiol.* **119**, 695–710 (2023).

45. R. Muñoz-Planillo, P. Kuffa, G. Martínez-Colón, B. L. Smith, T. M. Rajendiran, G. Núñez, K+ Efflux Is the Common Trigger of NLRP3 Inflammasome Activation by Bacterial Toxins and Particulate Matter. *Immunity* **38**, 1142–1153 (2013).

46. A. J. Trzeciak, W. S. Rojas, Z.-L. Liu, A. S. Krebs, Z. Wang, P. H. V. Saavedra, I. C. Miranda, A. Lipshutz, J. Xie, C.-L. Huang, M. Overholtzer, M. S. Glickman, C. N. Parkhurst, T. Vierbuchen, C. D. Lucas, J. S. A. Perry, WNK1 enforces macrophage lineage fidelity. *bioRxiv*, 2023.04.26.538482 (2023).

47. H. Genth, S. Pauillac, I. Schelle, P. Bouvet, C. Bouchier, C. Varela-Chavez, I. Just, M. R. Popoff, Large clostridial glucosylating toxins substrate specifcity. *Cell. Microbiol.* **16**, 1706–1721 (2014).

48. E. C. Freund, J. Y. Lock, J. Oh, T. Maculins, L. Delamarre, C. J. Bohlen, B. Haley, A. Murthy, Efficient gene knockout in primary human and murine myeloid cells by non-viral delivery of CRISPR-Cas9. *J. Exp. Med.* **217**, e20191692 (2020).

49. J. L. Schmid-Burgk, T. Schmidt, M. M. Gaidt, K. Pelka, E. Latz, T. S. Ebert, V. Hornung, OutKnocker: a web tool for rapid and simple genotyping of designer nuclease edited cell lines. *Genome Res.* **24**, 1719–1723 (2014).

50. S. Burger, H. Tatge, F. Hofmann, H. Genth, I. Just, R. Gerhard, Expression of recombinant Clostridium difficile toxin A using the Bacillus megaterium system. *Biochem Bioph Res Co* **307**, 584–588 (2003).

Acknowledgments: We thank H. Tatge for purification of the different *C.difficile* toxins. We thank the Microscopy Core Facility and Flow Cytometry Core Facility at the University of Bonn for providing help, service and devices. We thank Dr. Andreas Lindner for assistance with analysis of the sodium imaging data. We thank Prof. Stefan Matile and Lea Assies for the EE-flipper dye, Prof. Bernardo Franklin for reagents and the CASY cell analyser, Prof. Veit Hornung for the BLaER1 cells, Prof. Feng Shao for the LFn-PrgI construct, Dr. David Fußböller and Prof. Matthias Geyer for production of the LFn-PrgI. We thank Dr. Matthieu Piel, Dr. Nicolas Manel, Dr. Felix D. Weiss and Dr. Tomasz Prochnicki for scientific discussions.

Funding:

Deutsche Forschungsgemeinschaft (DFG, German Research Foundation) TRR237 (project-ID 369799452) (EL)

Deutsche Forschungsgemeinschaft (DFG, German Research Foundation) SFB1454 (project-ID 432325352) (EL)

Deutsche Forschungsgemeinschaft (DFG, German Research Foundation) SFB1403 (project-ID 414786233) (EL)

Germany's excellence strategy – EXC2151 (project-ID 390873048) (EL)

Deutsche Forschungsgemeinschaft (DFG, German Research Foundation) GE1017/5-1 (RG)

Helmholtz-Gemeinschaft, Zukunftsthema 'Immunology and Inflammation' (ZT-0027) (EL)

Author contributions:

Conceptualization: MSJM

Methodology: MSJM, GH, JH

Investigation: MSJM, AA, SR, GH, PW, RK, FD, JS

Visualization: MSJM, GH, JH

Resources: RG

Funding acquisition: EL, RG

Supervision: MSJM, DW, EL

Writing – original draft: MSJM

Writing – review & editing: MSJM with input from all authors

Competing interests: Eicke Latz is co-founder and consultant of IFM Therapeutics, DiosCure Therapeutics and Odyssey Therapeutics. The other authors declare no competing interests.

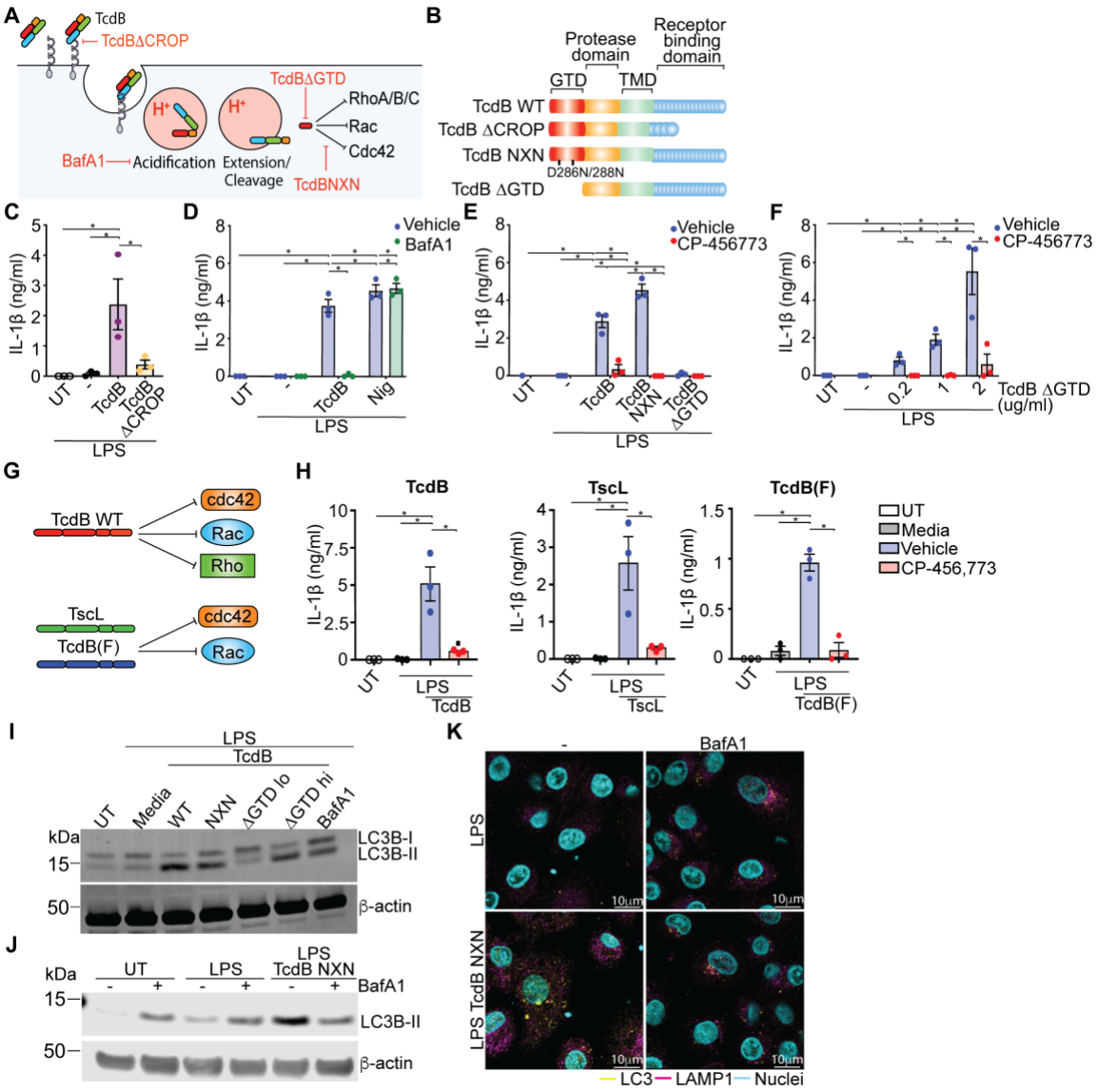
A
TcdB
TcdBΔCROP
TcdBΔGTD
RhoA/B/C
Rac
Cdc42
BafA1
Acidification
Extension/
Cleavage
TcdBNXN
B
Protease domain
Receptor binding domain
GTD
TMD
TcdB WT
TcdB ΔCROP
TcdB NXN
D286N/288N
TcdB ΔGTD
C
IL-1β (ng/ml)
UT
TcdB
TcdB ΔCROP
LPS
D
Vehicle
BafA1
Nig
E
CP-456773
TcdB NXN
TcdB ΔGTD
F
TcdB ΔGTD (ug/ml)
G
TcdB WT
cdc42
Rac
Rho
TscL
TcdB(F)
H
TcdB
TscL
TcdB(F)
Media
I
kDa
15
50
LC3B-I
LC3B-II
β-actin
ΔGTD lo
ΔGTD hi
J
K
BafA1
10μm
LC3
LAMP1
Nuclei

785

786

787

Fig 1. Activation of NLRP3 by TcdB requires receptor mediated uptake and endosomal acidification

A) TcdB intoxication pathway **B)** TcdB variants used. IL-1β release from LPS-primed hMDM incubated with **C)** TcdB or TcdB ΔCROP **D)** TcdB or nigericin after BafA1 pre-treatment (200 nM, 15 min) **E)** TcdB, TcdB NXN or TcdB ΔGTD (20 ng/ml) **F)** TcdB ΔGTD. **G)** TcdB, TcdB(F) and TscL substrate specificity. LPS-primed **H)** IL-1β release from hMDM pretreated with CP-456,773 or colchicine, then incubated with TcdB, TcdB(F) or TscL. **I)** Immunoblot of LC3B or actin in LPS-primed hMDM treated with the different toxins for 45 min. **J)** Immunoblot of LC3B or actin in LPS-primed hMDM treated +/- TcdB NXN in the presence or absence of BafA1, which was included 30 min post addition of TcdB NXN. **K)** LSC images of LPS-primed hMDM treated with TcdB NXN +/- BafA1 stained for LC3 (green) and LAMP1 (red). In all cases mean and SEM from 3 donors are shown, each point represents one donor. Immunoblot and imaging representative of 3 independent experiments. *$p<0.05$, only significant differences annotated

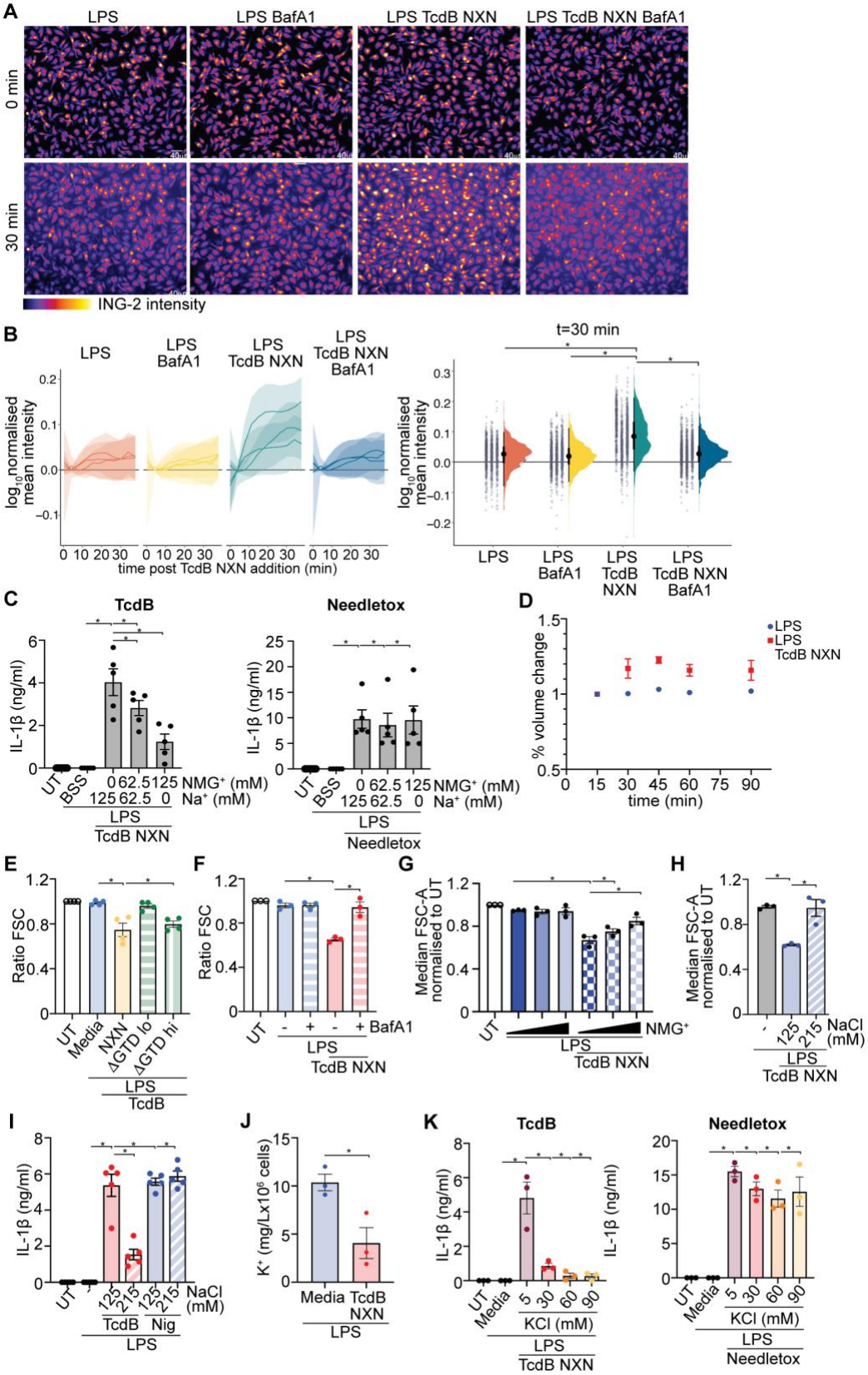
A
LPS
LPS BafA1
LPS TcdB NXN
LPS TcdB NXN BafA1
0 min
30 min
ING-2 intensity
B
LPS
LPS BafA1
LPS TcdB NXN
LPS TcdB NXN BafA1
log10 normalised mean intensity
time post TcdB NXN addition (min)
t=30 min
C
TcdB
Needletox
IL-1β (ng/ml)
NMG+ (mM)
Na+ (mM)
UT
BSS
LPS
TcdB NXN
Needletox
D
% volume change
time (min)
LPS
LPS TcdB NXN
E
Ratio FSC
UT
Media
NXN
ΔGTD lo
ΔGTD hi
LPS
TcdB
F
Ratio FSC
BafA1
LPS
TcdB NXN
G
Median FSC-A normalised to UT
NMG+
LPS
TcdB NXN
H
Median FSC-A normalised to UT
NaCl (mM)
LPS
TcdB NXN
I
IL-1β (ng/ml)
NaCl (mM)
TcdB
Nig
LPS
J
K+ (mg/Lx10^6 cells)
Media
TcdB NXN
LPS
K
TcdB
Needletox
IL-1β (ng/ml)
KCl (mM)
LPS
TcdB NXN
Needletox

803

Fig 2. TcdB triggers cytosolic sodium influx and cell swelling to trigger potassium-dependent NLRP3 activation

A) WF images of LPS-primed, ING-2 loaded hMDM stimulated with TcdB NXN +/- pre-incubation with BafA1. **B)** Quantitation of ING-2 intensity normalized per cell. Each line represents the mean (solid line) and S.D. (shaded area) for one experimental replicate. The per cell quantitation was graphed from the normalized values at t=30 min. **C)** IL-1β release from LPS-primed hMDM incubated with TcdB or Needletox in Na^+ or NMG^+ containing BSS. **D)** Relative cell diameter of LPS-primed hMDM +/- TcdB NXN. Median FSC of LPS-primed hMDM treated with **E)** TcdB NXN, TcdB ΔGTD lo (20 ng/ml), TcdB ΔGTD hi (1 μg/ml) or **F)** pretreated with BafA1 and normalised to UT hMDM. **G)** Normalised median FSC of LPS-primed hMDM stimulated with TcdB NXN in Na^+ or NMG^+ BSS or **H)** in BSS with 125 or 215 mM NaCl. **I)** IL-1β release from LPS-primed hMDM incubated with TcdB NXN or nigericin in BSS with 125 or 215 mM NaCl. **J)** [K^+] from LPS-primed hMDM +/- TcdB NXN. **K)** IL-1β release from LPS-primed hMDM incubated with TcdB NXN or needletox in BSS with increasing concentrations of KCl. Mean and SEM from 3-5 donors shown for C) – K), each point represents one donor. A), D), E), H), I) and J) were performed in the presence of CP-456,773. *$p<0.05$, only significant differences annotated.

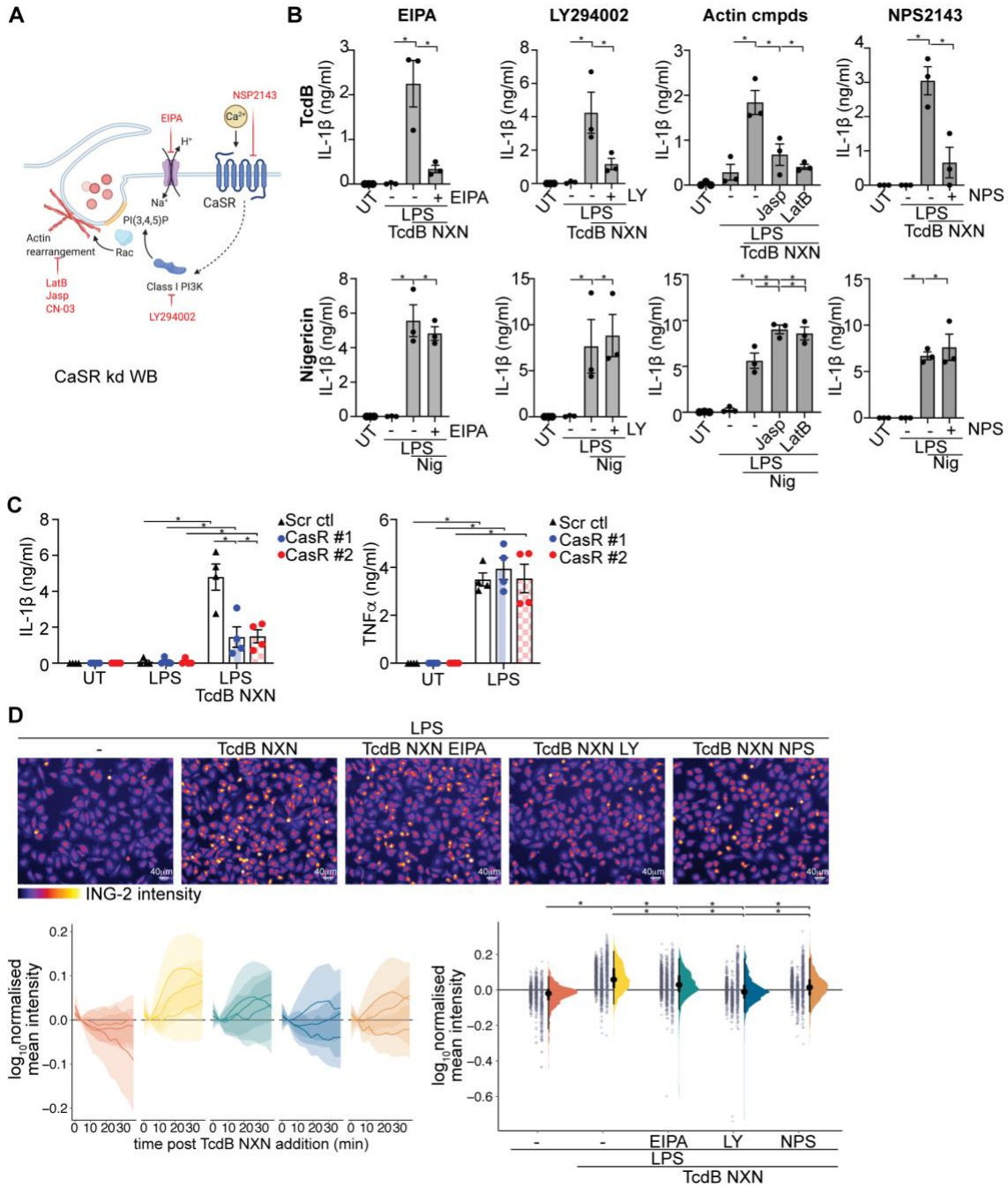
A
NSP2143
EIPA
Ca2+
H+
Na+
CaSR
PI(3,4,5)P
Actin rearrangement
Rac
LatB
Jasp
CN-03
Class I PI3K
LY294002
CaSR kd WB
B
EIPA
LY294002
Actin cmpds
NPS2143
TcdB
Nigericin
IL-1β (ng/ml)
UT
LPS
TcdB NXN
Nig
Jasp
LatB
C
Scr ctl
CasR #1
CasR #2
IL-1β (ng/ml)
TNFα (ng/ml)
D
LPS
TcdB NXN
TcdB NXN EIPA
TcdB NXN LY
TcdB NXN NPS
ING-2 intensity
log10 normalised mean intensity
time post TcdB NXN addition (min)
EIPA
LY
NPS

823

824

Fig 3. TcdB-mediated NLRP3 activation and cytosolic sodium accumulation requires macropinocytosis

A) The known processes required for macropinocytosis and their inhibitors. **B)** IL-1β release from UT or LPS-primed hMDM pre-incubated with EIPA (20 μM), LY294002 (10 μM), Jasplakinolide (0.5 μM), Latrunculin B (2 μM) or NPS2143 (5 μM) for 30 min, then treated with either TcdB NXN (20 ng/ml) or nigericin (8 μM) for 2h. **C)** IL-1β release and TNFα secretion from UT or LPS-primed hMDM electroporated with CaSR targeting or scrambled (scr) siRNA treated with TcdB NXN (20 ng/ml). **D)** WF images of LPS-primed, ING-2 loaded hMDM stimulated with TcdB NXN +/- pre-incubation with macropinocytosis inhibitors as listed above, t=30min. Quantitation of ING-2 intensity normalized per cell. Each line represents the mean (solid line) and S.D. (shaded area) for one experimental replicate. The per cell quantitation is from at t=30 min. Mean and SEM for 3-4 donors shown, each point represents one donor. *$p<0.05$, only significant differences annotated.

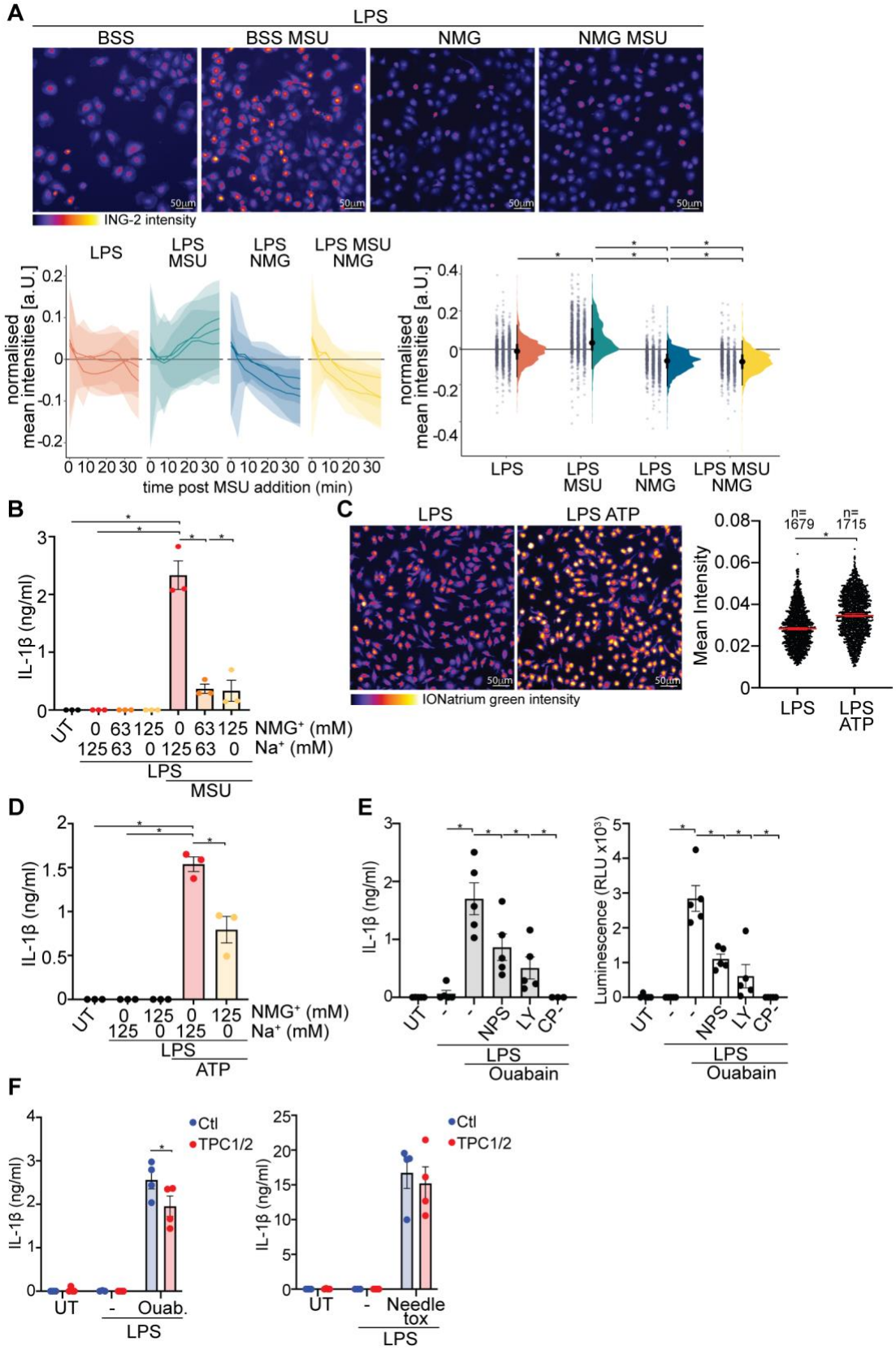
A
LPS
BSS
BSS MSU
NMG
NMG MSU
50µm
ING-2 intensity
LPS
LPS MSU
LPS NMG
LPS MSU NMG
normalised mean intensities [a.U.]
time post MSU addition (min)
B
IL-1β (ng/ml)
UT
NMG+ (mM)
Na+ (mM)
LPS
MSU
C
LPS
LPS ATP
IONatrium green intensity
Mean Intensity
n= 1679
n= 1715
D
IL-1β (ng/ml)
ATP
E
IL-1β (ng/ml)
Luminescence (RLU x10³)
NPS
LY
CP-
Ouabain
F
Ctl
TPC1/2
IL-1β (ng/ml)
Ouab.
Needle tox

840

Fig 4. Cytosolic sodium influx is a common event for particulate and non-particulate activators of NLRP3

A) WF images and quantitation of LPS-primed, ING-2 loaded hMDM stimulated with MSU crystals in Na^+ or NMG^+ containing BSS. ING-2 intensity normalized per cell. Each line represents the mean (solid line) and S.D. (shaded area) for one experimental replicate. The per cell quantitation is from at t=25 min. **B)** IL-1β release from LPS-primed hMDM incubated with MSU in Na^+ or NMG^+ containing BSS. **C)** WF images and quantitation of LPS-primed ING-2 loaded hMDM stimulated with ATP for 5 min. **D)** IL-1β release from LPS-primed hMDM incubated with ATP in Na^+ or NMG^+ containing BSS. **E)** IL-1β release from UT or LPS-primed hMDM pre-incubated with LY294002 (10 μM) or NPS2143 (5 μM) for 30 min, then treated with ouabain (0.5 mM). **F)** IL-1β release from control or TPC1/2 knock out hMDM treated with ouabain (0.5 mM) or needletox (20 ng/ml). Mean and SEM for 3-4 donors shown, each point represents one donor. A) and C) were performed in the presence of CP-456,773. *$p<0.05$, only significant differences annotated.

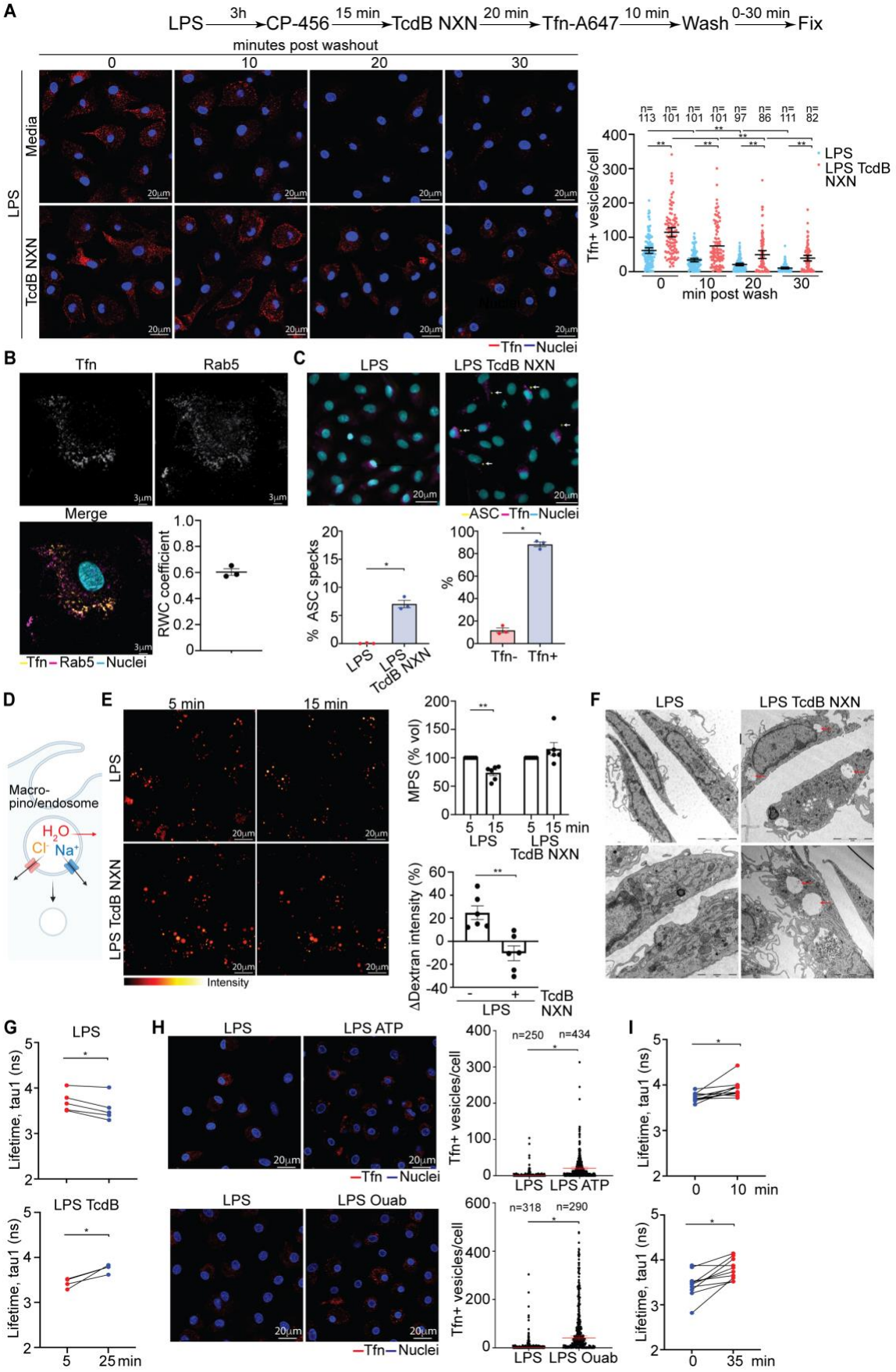
A
LPS 3h CP-456 15 min TcdB NXN 20 min Tfn-A647 10 min Wash 0-30 min Fix
minutes post washout
0 10 20 30
LPS
Media
TcdB NXN
Tfn+ vesicles/cell
min post wash
LPS
LPS TcdB NXN
Tfn Nuclei
B
Tfn
Rab5
Merge
RWC coefficient
Tfn Rab5 Nuclei
C
LPS
LPS TcdB NXN
ASC Tfn Nuclei
% ASC specks
%
Tfn-
Tfn+
D
Macro-pino/endosome
H2O
Cl-
Na+
E
5 min
15 min
LPS
LPS TcdB NXN
Intensity
MPS (% vol)
ΔDextran intensity (%)
TcdB NXN
F
LPS
LPS TcdB NXN
G
LPS
LPS TcdB
Lifetime, tau1 (ns)
5 25 min
H
LPS
LPS ATP
LPS Ouab
Tfn Nuclei
n=250 n=434
n=318 n=290
I
0 10 min
0 35 min

855

Fig 5. TcdB inhibits osmotic resolution of endosomes to enable NLRP3 inflammasome activation

A) LSC images and quantitation of Tfn-A647 pulse-chase in LPS-primed hMDM treated +/- TcdB NXN. Mean and 95% CI shown, each dot represents one cell, data is from pooled from 3 experimental replicates. **B)** LSC images and Rank-Weighted Colocalization (RWC) coefficient analysis of Tfn-A647 and Rab5 in LPS-primed-hMDM treated +/- TcdB NXN. Each point represents the mean RWC value for each experimental replicate, approx. 50 cells analyzed per donor. **C)** WF images and quantitation of ASC-speck$^+$ and Tfn$^+$ hMDM LPS-primed, pre-incubated with VX-765 and treated +/- TcdB NXN. Mean and SEM from 3 independent donors, approx. 1500 cells analyzed/donor. **D)** Process of osmotic resolution of macropinosomes. **E)** LSC images and analysis of LPS-primed hMDM +/- TcdB NXN pulsed with 70 kDa Oregon green (OG) labelled dextran and 200 U/ml M-CSF for 4 min, then washed and imaged over time. Each dot represents the average volume and intensity for an experimental repeat, mean and SEM shown. **F)** TEM of LPS primed hMDM incubated with TcdB NXN (45 min), representative of 3 independent donors. **G)** FLIM analysis of LPS-primed, EE-flipper (2 μM) loaded hMDM +/- TcdB NXN, n=3, mean shown. **H)** LSC images and quantitation of hMDM with Tfn$^+$ vesicles in LPS-primed hMDM +/- ATP (5 mM) or ouabain (0.5 mM). Mean and 95% CI shown, data pooled from 3 independent experiments **I)** FLIM analysis of LPS-primed, EE-flipper (2 μM) loaded hMDM treated as in (H), each point represents one technical repeat, representative of 3 independent experiments. In all experiments except C) hMDM were pre-incubated with CP-456,773. *$p<0.05$, only significant differences annotated.

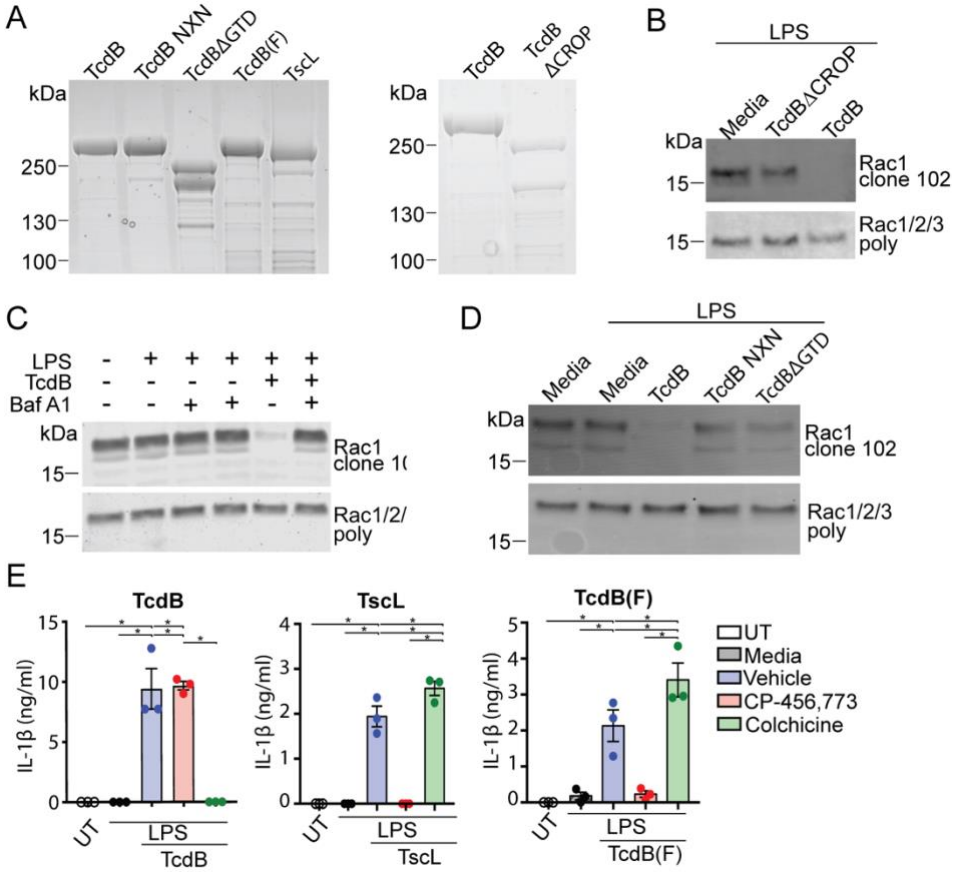

Fig. S1.

A) Coomassie stained SDS-PAGE gel characterizing TcdB, TcdB mutants and TscL. Immunoblots of cell lysate from hMDM treated as in **B)** Fig 1C or **C)** Fig 1D or **D)** Fig 1E probed for TcdB-modified Rac (Rac antibody clone 102) or for total Rac (Rac1/2/3 poly) to assess TcdB-mediated Rac2/3 modification. **E)** IL-1β release from monocytes (1 ng/ml, 3 h) pretreated with CP-456,773 (2.5 μM, 15 min) or colchicine (2 μM, 15 min), then incubated with TcdB, TcdB(F) (20 ng/ml) or TscL (100 ng/ml). Coomassie gel n=1, immunoblots are representative of 3 independent experiments. Statistics indicates significance by one-way ANOVA, *p<0.05, only significant differences annotated.

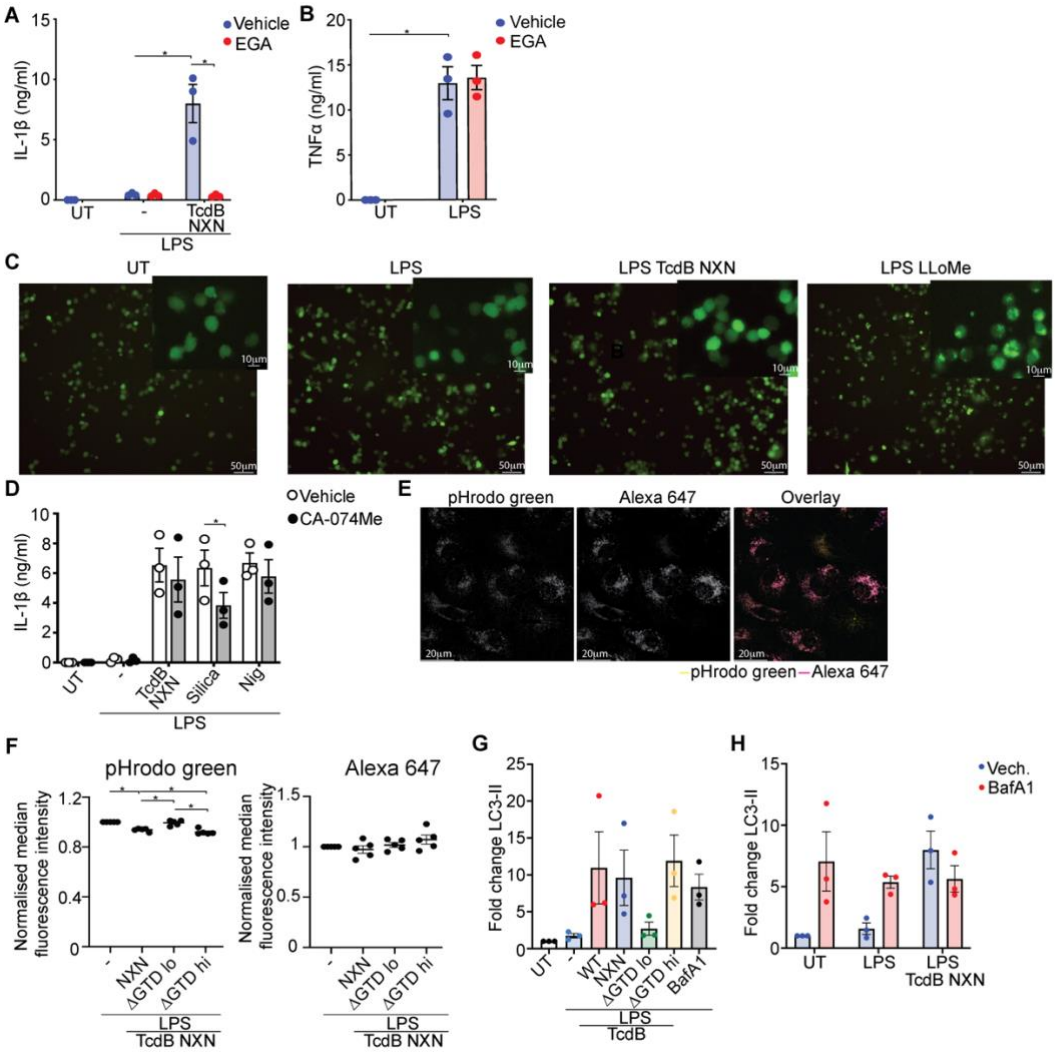

Fig. S2.

A) IL-1β release from UT or LPS-primed hMDM pre-incubated with EGA (5 μM, 30 min), then treated with TcdB NXN (20 ng/ml, 2 h). **B)** TNFα release from UT or LPS-primed hMDM pre-incubated with EGA (5 μM, 2.5 h). **C)** WF images of trans-differentiated BLaER1 cells expressing a Gal-8-mCitrine fusion protein were primed with LPS (100 ng/ml, 3h) and treated with either TcdB NXN (20 ng/ml) or LLoMe (0.5 mM, 30 min). Representative of 3 independent experiments. **D)** IL-1β release from UT or LPS-primed hMDM pre-incubated with CA-047Me (0.5 μM, 30 min), then treated with either TcdB NXN (20 ng/ml), silica crystals (100 μg/ml) or nigericin (8

μM) for 2h. **E)** LSC images of hMDM loaded with both dextrans. **F)** MFI of pHrodo green- or Alexafluor 647-coupled 10 kDa dextrans from LPS-primed hMDM treated with TcdB variants or BafA1. MFI was normalized to LPS alone. **G)** Analysis of LC3-II levels from immunoblot in Fig. 1J. **H)** Analysis of LC3-IIB levels from immunoblot in Fig. 1K. Mean and SEM shown for 3-5 independent donors shown. hMDM in (C), (D), (F), (H) and (J) were preincubated with CP-456,773 prior to addition of TcdB. Statistics indicates significance by (A, B, D) students two-tailed t-test or (F, G) one-way ANOVA, *$p<0.05$, only significant differences annotated.

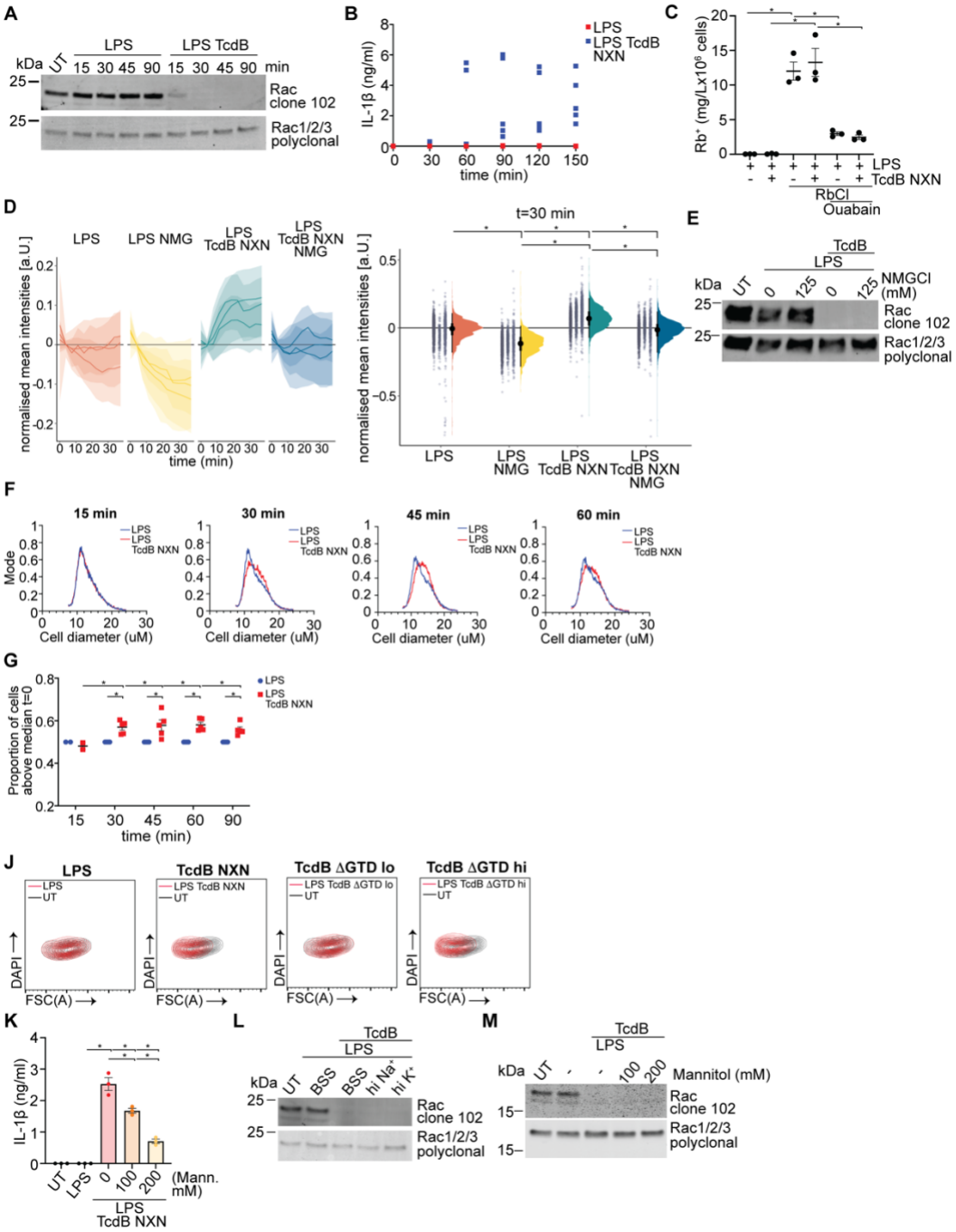

Fig. S3.

A) Rac2/3 from lysate and **B)** IL-1β release and assessed from cell-free supernatant in LPS-primed hMDM incubated with TcdB for various time points. Mean and SEM of 5 independent experiments shown, immunoblot representative of 3 independent experiments. **C)** Rb^+ uptake in LPS-primed hMDM +/- TcdB NXN +/- ouabain (2.5 mM) for 1h. **D)** Rac2/3 from LPS-primed hMDM +/- TcdB in Na^+ or NMG^+ containing BSS.

E) Quantitation of ING-2 intensity in LPS-primed hMDM treated as listed and normalized per cell. Each line represents the mean (solid line) and SD (shaded area) for one experimental replicate. The per cell quantitation is from at t=30 min. **F)** Representative histograms of the cell diameter of hMDM +/- TcdB NXN as measured by the CASY cell analyser. **G)** Proportion of LPS-primed hMDM treated with TcdB NXN with a median diameter greater than LPS treated hMDM. **H)** Sample density blots from Fig 2E. **I)** IL-1β release from LPS-primed hMDM incubated with TcdB NXN in media with increasing concentrations of mannitol. **J)** Immunoblot of hMDM treated as indicated. Mean and SEM shown for three independent donors, immunoblots representative of (A) three or (D, L) two independent experiments. hMDM were pre-incubated with CP-456,773 in (A), (C), (E), (F), (G), (I) and (J) prior to addition of the inflammasome stimulus. Statistics indicates significance by (C, D, K) one-way or (G) two-way ANOVA, *$p<0.05$, only significant differences annotated.

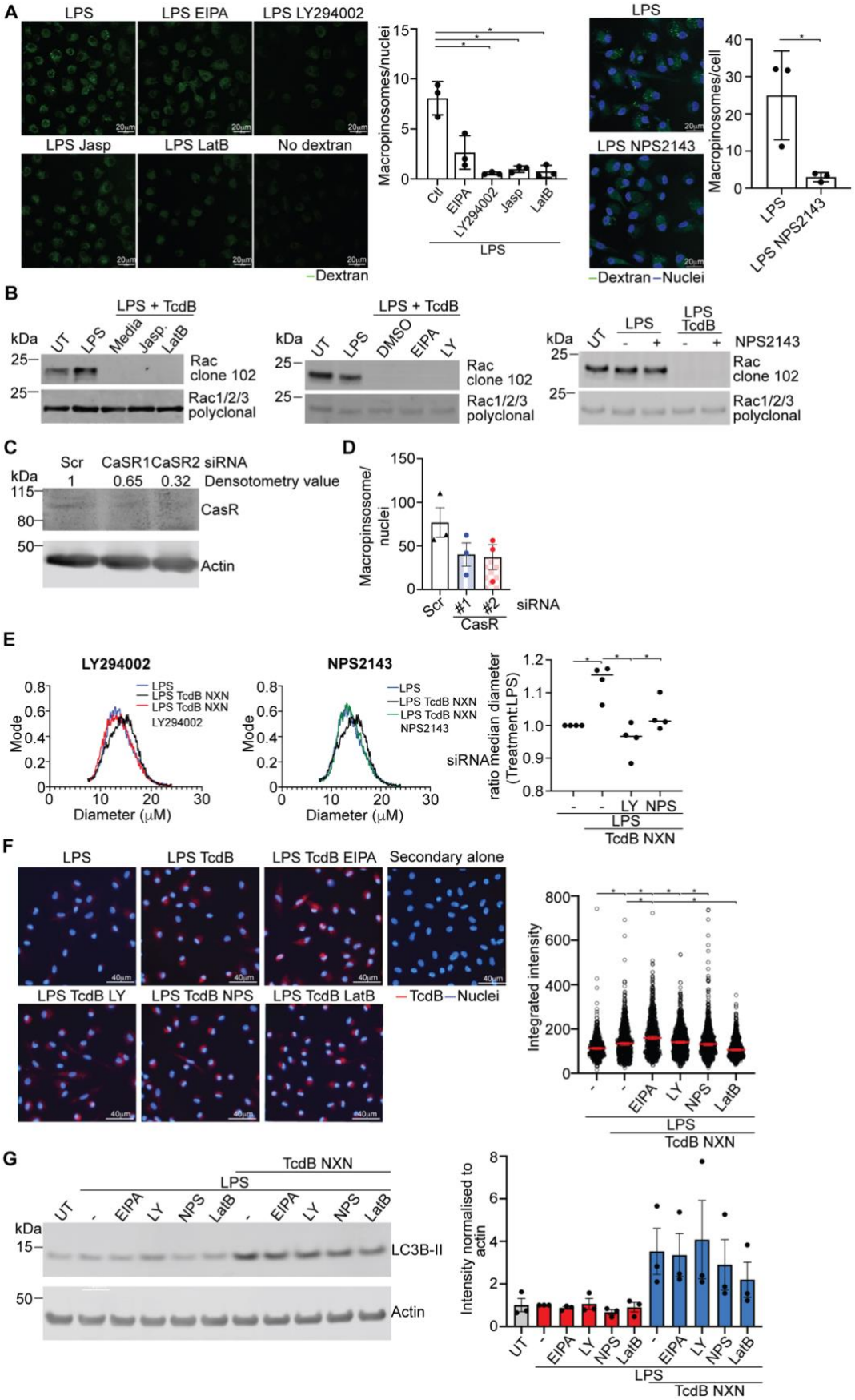
A
LPS
LPS EIPA
LPS LY294002
LPS Jasp
LPS LatB
No dextran
Dextran
Macropinosomes/nuclei
Ctl
EIPA
LY294002
Jasp
LatB
LPS
LPS NPS2143
Dextran Nuclei
Macropinosomes/cell
B
LPS + TcdB
kDa
UT
LPS
Media
Jasp.
LatB
Rac clone 102
Rac1/2/3 polyclonal
DMSO
EIPA
LY
NPS2143
C
Scr
CaSR1
CaSR2 siRNA
1
0.65
0.32
Densotometry value
CasR
Actin
D
Macropinsosome/ nuclei
Scr
#1
#2
siRNA
CasR
E
LY294002
NPS2143
LPS
LPS TcdB NXN
Mode
Diameter (μM)
ratio median diameter (Treatment:LPS)
siRNA
LY
NPS
TcdB NXN
F
LPS TcdB
LPS TcdB EIPA
Secondary alone
LPS TcdB LY
LPS TcdB NPS
LPS TcdB LatB
TcdB Nuclei
Integrated intensity
G
TcdB NXN
LC3B-II
Intensity normalised to actin

Fig. S4.

A) LSC images and analysis of LPS-primed hMDM incubated with EIPA (20 μM), LY294002 (10 μM), Jasplakinolide (0.5 μM), Latruculin B (2 μM) or NPS2143 (5 μM) for 30 min, then incubated with OG-labeled 70kDa dextran for 15 min (25 μg/ml). The mean number of macropinosomes was quantitated for each condition (n>100 cells per condition). n=3, mean and SEM shown. **B)** Immunoblots from hMDM treated with inhibitors as in Fig 5A, B or C, then incubated with TcdB (20 ng/ml) for 45 min before lysis and assessment of Rac modification. Representative of three independent experiments. **C)** Immunoblot of CaSR or scr siRNA electroporated hMDM. **D)** Macropinosomes per nuclei in hMDM treated as in Fig. 3C. **E)** Median cell diameter for LPS-primed hMDM with either LY294002 or NPS2143 and VX-765 analysed after 40 min TcdB NXN stimulation normalized to the median cell diameter in the LPS condition. **F)** WF images and analysis of TcdB uptake in LPS-primed hMDM incubated with inhibitors as in (A) and incubated with TcdB NXN for 45 min in the presence of CP-456,773. Mean and 95% CI shown. **G)** LC3B-II levels and quantitation in hMDM treated as in (D). Unless otherwise stated mean and SEM shown, each dot represents one donor. Immunoblots are representative of 3 independent experiments. Statistics indicates significance by (A, D, E) one-way ANOVA or (A, NPS2143) Students two-tailed t-test, *p<0.05, only significant differences annotated.

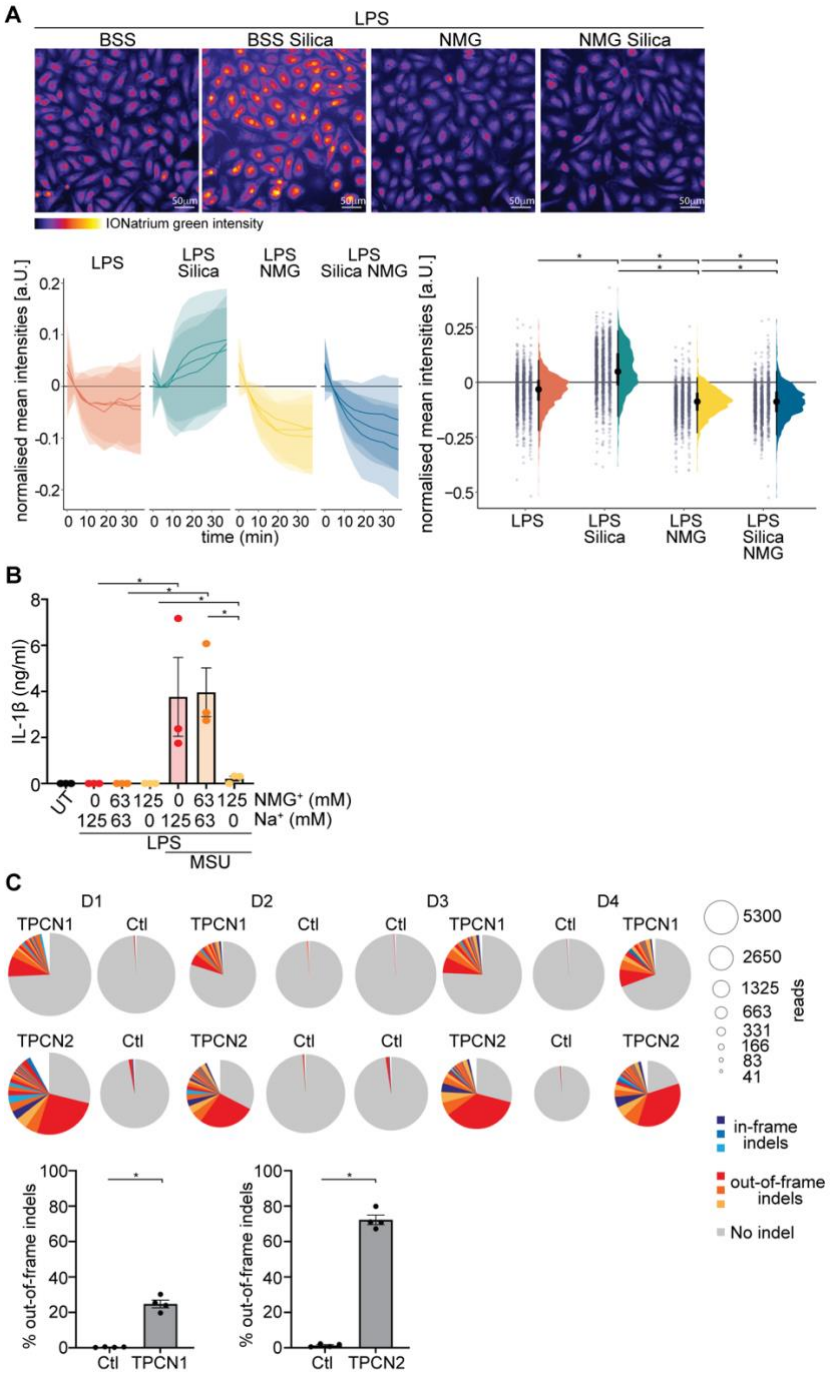

Fig. S5

A) WF images of LPS-primed, ING-2 loaded hMDM stimulated with Silica (100 μg/ml) on Na^+ or NMG^+ BSS. Quantitation of ING-2 intensity normalized per cell. Each line represents the mean (solid line) and SD (shaded area) for one experimental replicate. The per cell quantitation is from at t=25 min. **B)** IL-1β release from LPS-primed hMDM stimulated with Silica (100 μg/ml) on Na^+ or NMG^+ BSS. **C)** Out-of-frame indel

efficiency in hMDM transfected with Cas9-gRNA complexes targeting *TPCN1* or *TPCN2*. Mean and SEM shown, each dot represents one donor. Statistics indicates significance by (A, B) one-way ANOVA or (C) Student's t-test, *$p<0.05$, only significant differences annotated.

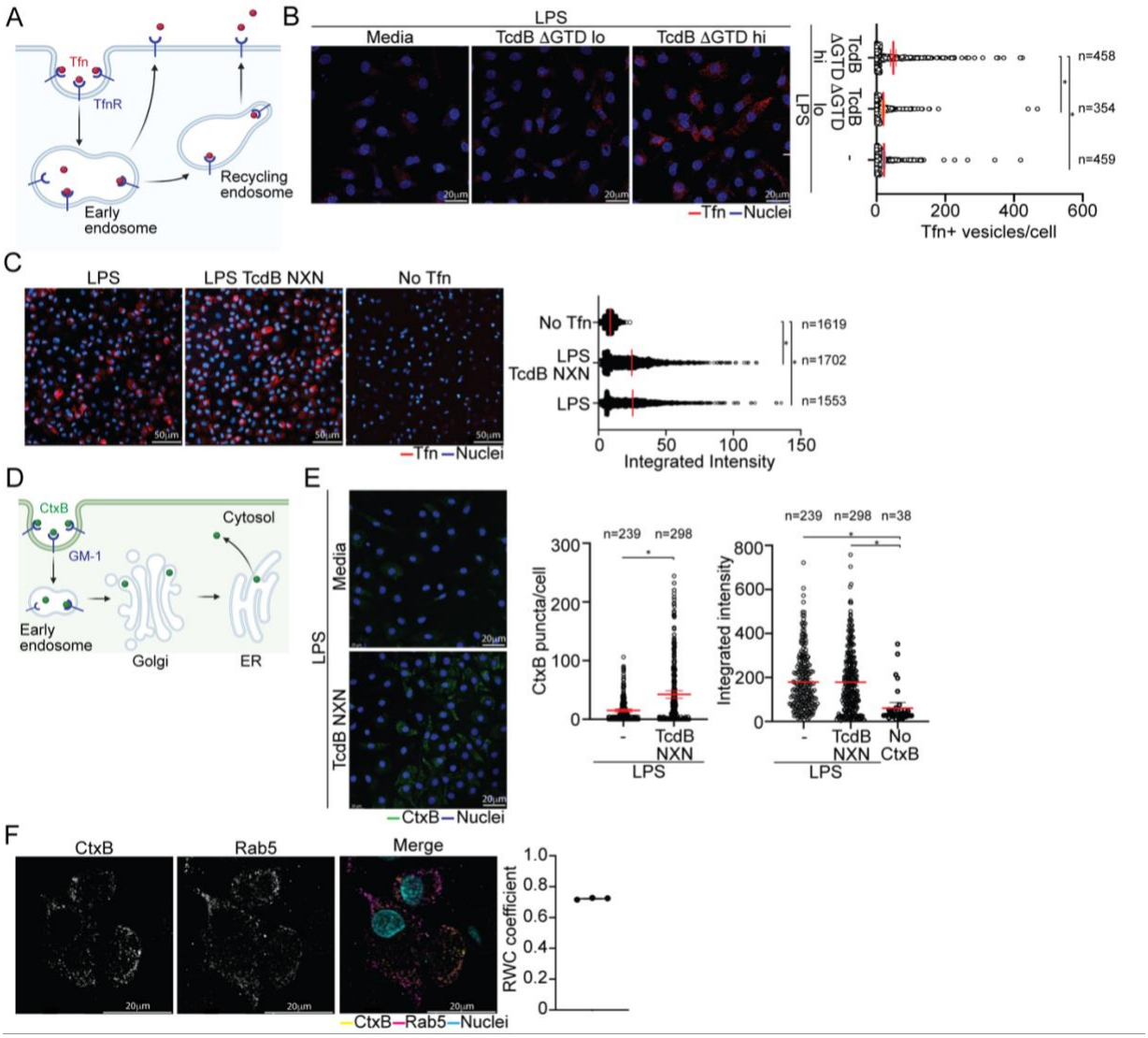

Fig. S6

A) Schematic of the Tfn trafficking pathway. **B)** LSC images and analysis of Tfn-A647 pulse-chase (chase period 30 min) in LPS-primed hMDM incubated with TcdBΔGTD lo (20 ng/ml) or hi (1 μg/ml). Each point represents one cell, data pooled from three independent experiments, mean and 95% CI. **C)** WF imaging and analysis of Tfn binding for LPS-primed hMDM, each dot represents 1 cell, mean and 95% CI shown. Representative of 2 independent experiments. **D)** Schematic of the CtxB trafficking pathway. **E)** LSC images and analysis of CtxB-A594 pulse-chase (pulse 10 min, chase period 30 min) in LPS-primed hMDM incubated with TcdB NXN preincubated with CP-

456,773. Data pooled from of 3 independent experiments, each point represents one cells, mean and 95% CI shown. **F)** LSC images and co-occurrence analysis of CtxB-A594 and Rab5 in LPS-primed, TcdB NXN treated hMDM. Mean and SEM shown, approx. 50 cells analysed per donor. Each dot represents the average RWC from one donor. Statistics indicates significance by (B, C, E) one-way ANOVA, *$p<0.05$, only significant differences annotated.

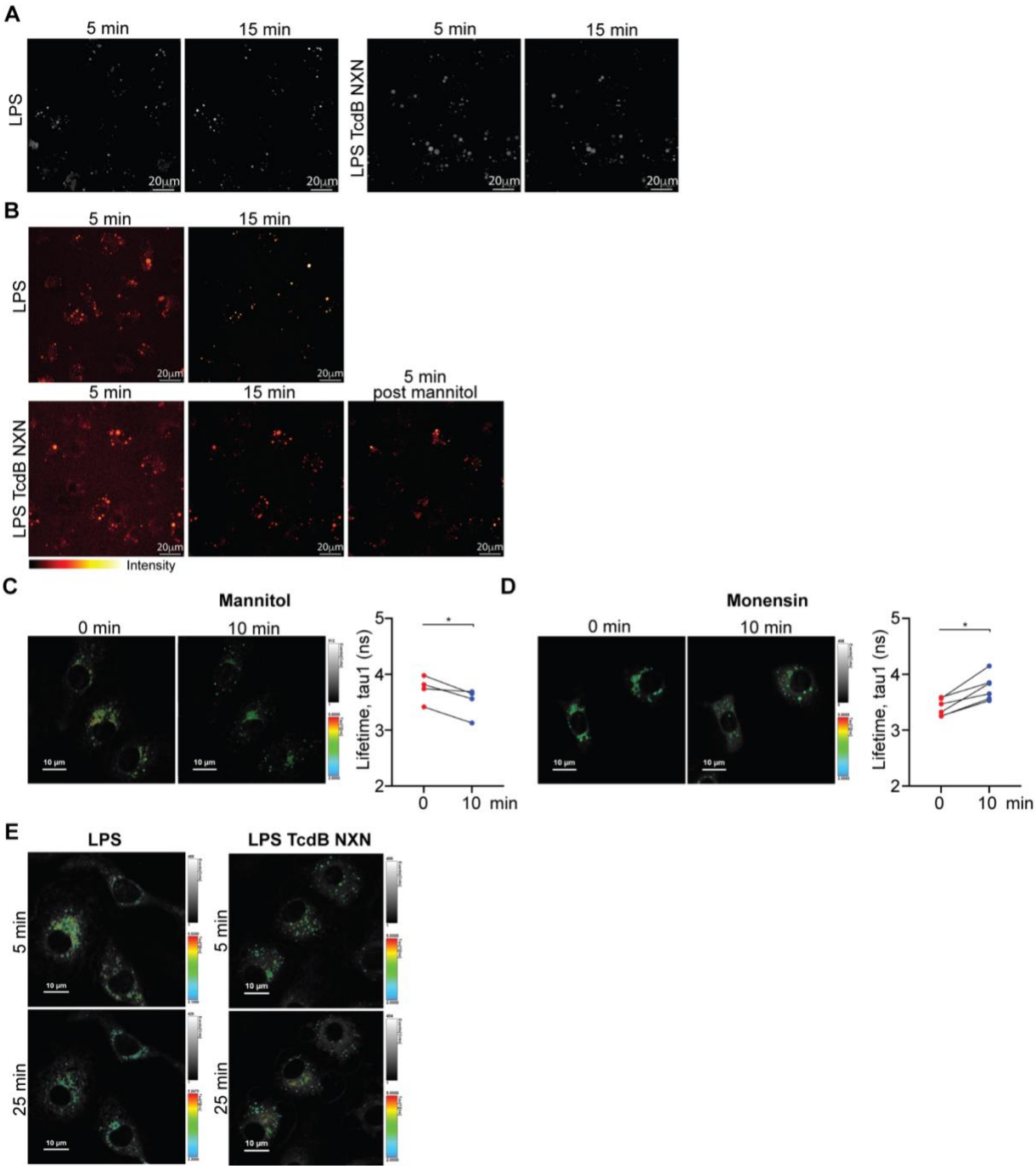

Fig. S7

A) Greyscale confocal images of the images shown in Fig 5E. **B)** hMDM treated as in Fig 4E, the LPS-primed, TcdB NXN treated hMDM pulsed with 0.25 M mannitol, then imaged for a further 5 min. Mean and SEM shown for 5 experimental repeats. FLIM images and analysis for EE-flipper (2 µM, 10 min) loaded, LPS-primed hMDM treated with **C)** mannitol (0.25 M), **D)** monensin (2 µM) for 10 min or TcdB for 25 min. Each

pair represents one experimental repeat. **E)** FLIM images for EE-flipper (2 μM, 10 min) loaded, LPS-primed hMDM treated as in Fig. 5G. Statistics indicates significance by (C, D) Students paired two-tailed t-test, *$p<0.05$, only significant differences annotated.

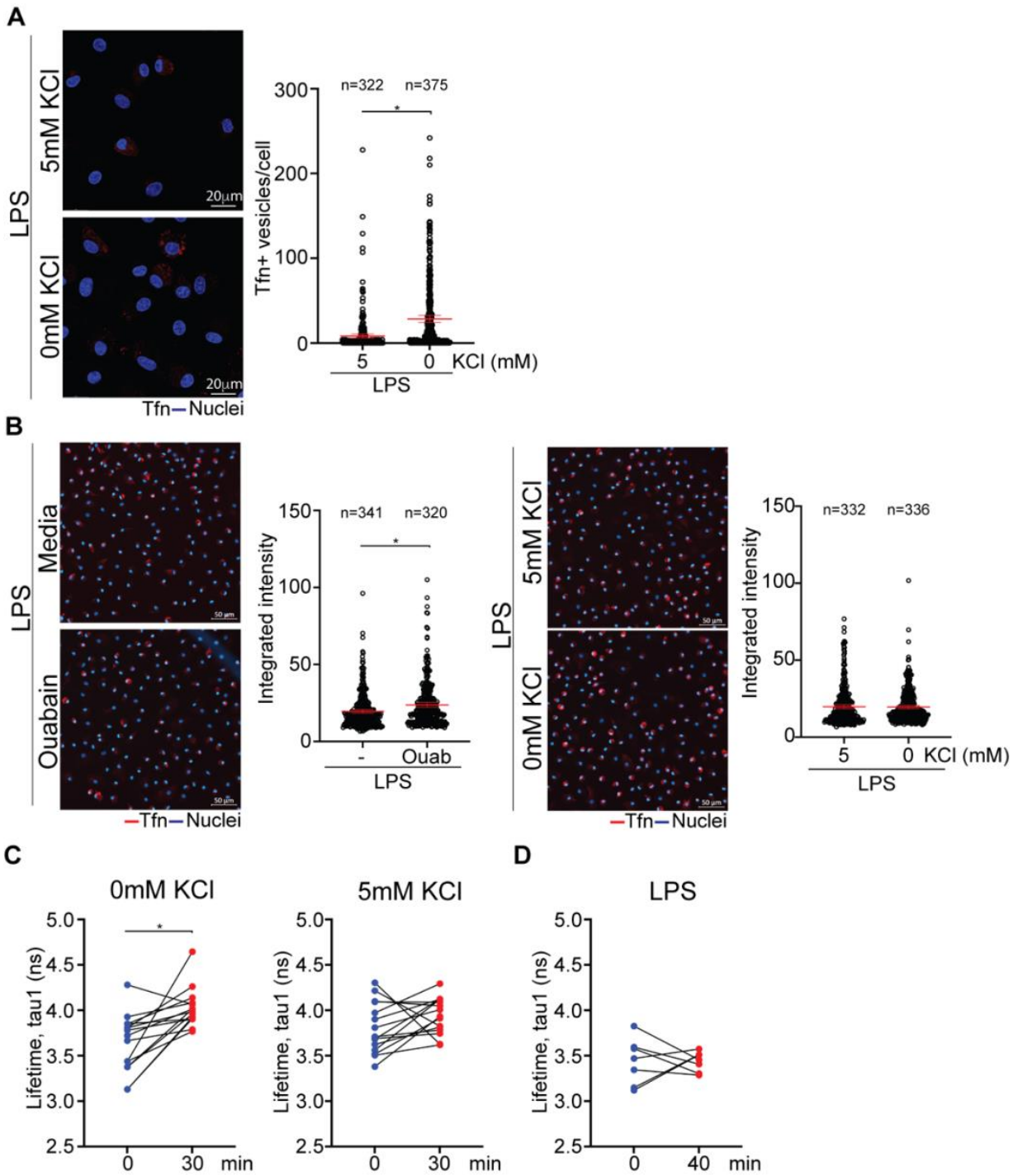

Fig. S8

A) LSC images of Tfn-A647 pulse-chase (pulse 10 min, chase 30 min) in LPS-primed hMDM pretreated with CP-456,773 and incubated in BSS/ K^+ free BSS for 30 min prior to pulse. Data pooled from three independent experiments, each point represents one

cell, mean and 95% CI shown. **B)** WF imaging and analysis of Tfn binding for LPS-primed hMDM +/- ouabain (0.5 mM, 30 min), or in BSS or K^+ free BSS (30 min). Each dot represents 1 cell, mean and 95% CI shown. Representative of 2 independent experiments. **C)** FLIM images and analysis for EE-flipper (2 μM, 10 min) loaded, LPS-primed hMDM treated with BSS or K^+ free BSS (30 min). Each pair represents one technical repeat, representative of 3 independent experiments. **D)** EE-flipper analysis for EE-flipper (2 μM, 10 min) loaded, LPS-primed hMDM (40 min). Each pair represents one technical repeat, representative of 2 independent experiments. Statistics indicates significance by (A, B) Students unpaired or (C) paired two-tailed t-test, *$p<0.05$, only significant differences annotated.

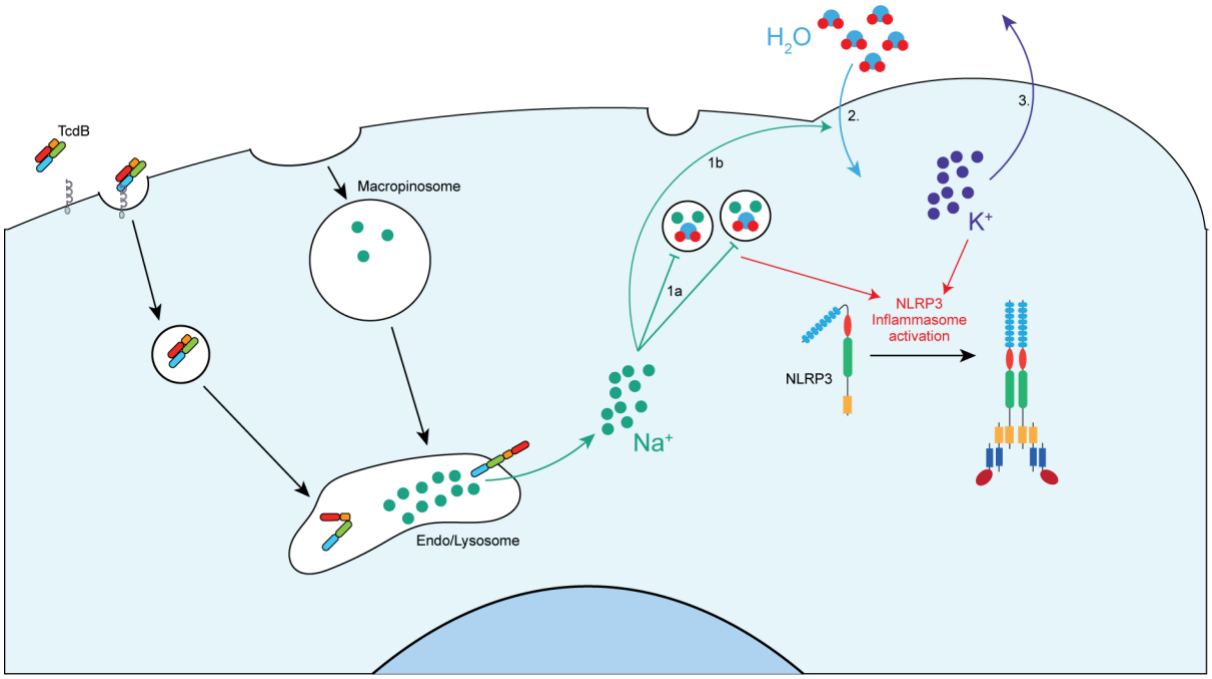

Fig. S9

Model of TcdB-mediated NLRP3 activation. TcdB is trafficked to the late endosome/ lysosome, where it enables translocation of sodium to the cytosol. Here the accumulated sodium blocks endocytic trafficking (1a) and triggers water influx (1b). Subsequent water influx triggers cell swelling (2) which in turn triggers potassium efflux (3), leading to NLRP3 inflammasome activation.

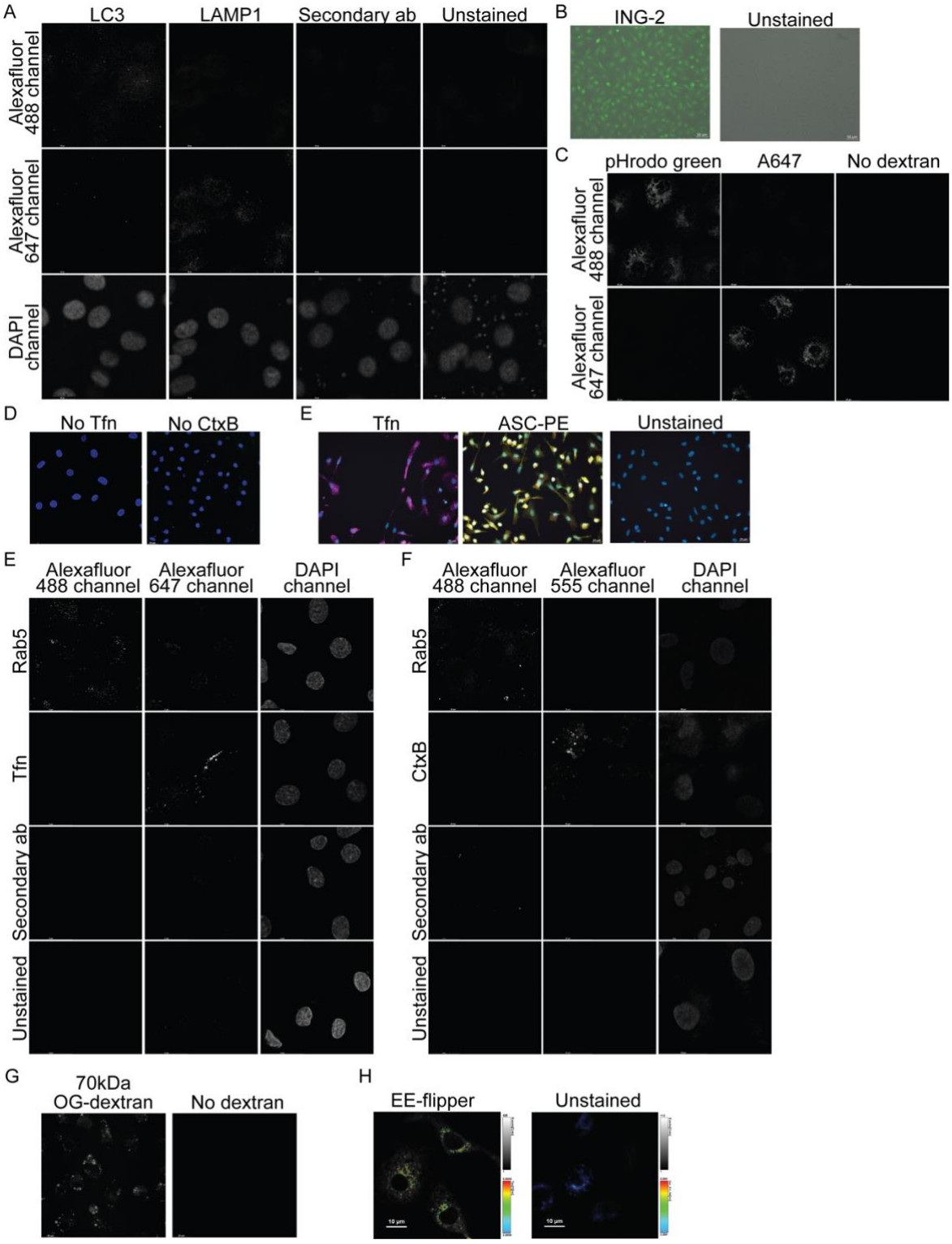

Fig. S10

Single color, secondary antibody alone and unloaded controls for **A)** Fig. 1L **B)** Fig. 2A **C)** Fig. S2E **D)** Fig. 5A, S6E **E)** Fig. 5C **F)** Fig. 5B **G)** Fig. S6F **H)** Fig. 5E, S7B **I)** Unstained control for all EE-flipper experiments.